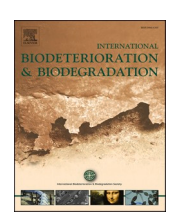
ELSEVIER

Contents lists available at ScienceDirect

# International Biodeterioration & Biodegradation

journal homepage: www.elsevier.com/locate/ibiod





# Biosynthesis of silver-based nanoparticles: Critical assessment of antimicrobial assays and diffusion kinetics analysis

António Carrapiço <sup>a,b</sup>, Manuel Pico <sup>c</sup>, Elisabete P. Carreiro <sup>d</sup>, Pedro Barrulas <sup>a,c</sup>, José Mirão <sup>a,e</sup>, Ana Teresa Caldeira <sup>a,c,f</sup>, Jorge Teixeira <sup>a,c</sup>, Luís Dias <sup>a,b</sup>, Maria Rosario Martins <sup>a,g,\*</sup>

- <sup>a</sup> HERCULES Laboratory and IN2PAST Associate Laboratory for Research and Innovation in Heritage, Arts, Sustainability and Territory, University of Évora, Palácio do Vimioso, Largo Marquês de Marialva, 8, 7000-809, Évora, Portugal
- b Institute for Research and Advanced Training (IIFA), University of Évora, Palácio do Vimioso, Largo Marquês de Marialva, 8, 7000-809, Évora, Portugal
- c Department of Chemistry and Biochemistry, ECT, University of Évora, Colégio Luís António Verney, Rua Romão Ramalho, 59, 7000-671, Évora, Portugal
- d LAQV-REQUIMTE, IIFA, University of Évora, Colégio Luís António Verney, Rua Romão Ramalho, 59, 7000-671, Évora, Portugal
- e Department of Geosciences, ECT, University of Évora, Colégio Luís António Verney, Rua Romão Ramalho, 59, 7000-671, Évora, Portugal
- <sup>f</sup> City University of Macau, Av. Padre Tomás Pereira Taipa, Macau
- g Department of Medical Sciences and Health, ESDH, University of Évora, Colégio Luís António Verney, Rua Romão Ramalho, 59, 7000-671, Évora, Portugal

#### ARTICLE INFO

#### Keywords: Silver nanoparticles (AgNPs) Biosynthesis Antimicrobial activity Disc diffusion assay Nanoparticle diffusion kinetics

#### ABSTRACT

Synthesis and application of nanoparticles (NPs) have shown promising results in various scientific fields due to their differentiating properties. However, current nanoparticle synthesis methods present environmental challenges. In this study biosynthesized silver nanoparticles (AgNPs) were produced from microbial culture supernatants as an alternative to traditional routes for controlling biodeteriogenic microorganisms in cultural heritage materials. The particles strongly inhibited cultural heritage colonizing bacteria and fungi, with minimum inhibitory concentrations ranging from 3 to 28 ppm. Kinetic analysis of disc diffusion assays revealed that inhibition zones correlate directly with silver ion release rates, rather than nanoparticle diffusion in agar. This led to a proposition of a simplified mechanistic model of Ag-based NPs behavior in disc diffusion assay. These findings carry broad implications - not only for the conservation of Cultural Heritage but also for diverse sectors, particularly human health - where accurate assessment of antimicrobial efficacy is paramount. To ensure accurate assessments, alternative methods should be standardized.

### 1. Introduction

Nanoparticles have a great variety of applications and properties, including color-tunable optics, enhanced mechanical or conductive performance, improve biomaterials properties (Wang et al., 2023), boost immunoassays sensitivity (Zhang et al., 2025), efficient photocatalysts, and high antimicrobial activity (Khan et al., 2019; Ogochukwu et al., 2024). Nanoparticle synthesis methods are broadly categorized into chemical, physical, and biological, each with their own advantages and disadvantages. Physical methods (mostly top-down approaches), typically do not involve chemical reagents or solvents, resulting in "cleaner" nanoparticles with high purity (Jagdeo, 2023; Al-Harbi and Abd-Elrahman, 2024). However, they often require specialized

equipment and high energy consumption. Chemical methods, by far the most used, offer good control, scalability and many functionalization options, but usually require the use of toxic or environmentally hazardous reagents and solvents (Vishwanath and Negi, 2021). Biological methods (biosynthesis), which use complex extracts from plants or supernatants from microorganisms, require less energy and avoid hazardous chemicals, reducing their environmental and economic impact, though they require more laborious isolation protocols (Ying et al., 2022).

Because there is an ever-increasing need for approaches that use less resources (Pérez-Hernández et al., 2021), and biosynthesis lowers energy input and eliminates most hazardous solvents, it directly advances the United Nations Sustainable Development Goals - especially SDG 9

<sup>\*</sup> Corresponding author. HERCULES Laboratory and IN2PAST - Associate Laboratory for Research and Innovation in Heritage, Arts, Sustainability and Territory, University of Évora, Palácio do Vimioso, Largo Marquês de Marialva, 8, 7000-809, Évora, Portugal E-mail address: mrm@uevora.pt (M.R. Martins).

(Industry, Innovation and Infrastructure) and SDG 12 (Responsible Consumption and Production) - while still producing functional metal nanoparticles. Also, recent works show that biosynthesized AgNPs can match or surpass the antimicrobial efficacy of traditional dry and wet chemistry routes while reducing life-cycle CO<sub>2</sub> emissions (compared with traditional methods) (Pourzahedi and Eckelman, 2015; Temizel-Sekeryan and Hicks, 2020; Han et al., 2025), therefore presenting itself as a better alternative, particularly for applications where high purity and precise functionalization control is not required.

One example of such applications is the control of microbiological contamination (biocontamination) of cultural heritage materials which might lead to its deterioration in a process referred to as biodeterioration (Camuffo et al., 2010). Cultural Heritage (CH) embodies the accumulated knowledge of generations and provides a foundation for identity, continuity, and future innovation (UNESCO, 1972; The European Council, 2006). Therefore, preserving CH by controlling microbiological contamination is crucial for ensuring the longevity of the knowledge it holds. There have been a few studies on the use of nanoparticles, particularly metal-based nanoparticles (mainly commercial or chemically synthesized), against the biocontamination of such materials with promising results regarding their antimicrobial potential against microorganisms isolated from cultural heritage materials (Franco-Castillo et al., 2021). However, these findings primarily rely on antimicrobial assays designed for clinical microbiology, which often involve organic antimicrobials, raising questions about their relevance to nanoparticle studies (Franco-Castillo et al., 2021; Gopal et al., 2018; Kourmouli et al.,

Despite the environmental advantages noted above, relatively few studies have (i) tested biosynthesized AgNPs against CH specific microorganisms (Franco-Castillo et al., 2021; Carrapiço et al., 2023) or (ii) evaluated whether standard diffusion assays correctly reflect ion-driven nanoparticle action (Gopal et al., 2018; Kourmouli et al., 2018). Addressing both issues is essential for delivering highly efficient antimicrobials with lower environmental impact for CH conservation. Accordingly, the present work couples microbiological supernatant syntheses with two main objectives: (i) measuring the efficacy of the resulting AgNPs against a panel of CH isolates and (ii) determining, through kinetic analysis, whether the disc diffusion assay faithfully captures their antimicrobial potential.

Thus, aiming to contribute to the conservation of CH by using innovative approaches that use less energy, produce fewer toxic wastes and reduce costs, we intended to synthesize Ag-based NPs with high antimicrobial potential, using supernatants of microbial cultures. This method stands out by leveraging microbe-derived components, potentially enhancing antimicrobial efficacy while reducing environmental impact. Following synthesis, Ag-based NPs were characterized (DLS, SEM-EDX, XRD, ICP-MS) and assayed against biodeteriogenic microorganisms previously isolated from contaminated CH objects. To assess the antimicrobial potential of the biosynthesized Ag-based NPs, minimum inhibitory concentration (MIC), post-exposure growth, and disc diffusion assays were used. Additionally, from kinetics analysis using a mathematical model that estimates silver ion release rates from AgNPs, new insights into the applicability of the disc diffusion method for assessing nanoparticle antimicrobial potential were revealed. Building on these findings and supported by earlier studies, a simplified mechanism was also proposed to explain how nanoparticles exert their antimicrobial effects in disc diffusion assays.

# 2. Materials and methods

# 2.1. Reagents and culture media

All chemicals were of analytical grade, and biological powders used for culture media preparation met microbiology standards. Chemicals and biological powders were used as received without any further purification: D(+)-glucose monohydrate and  $AgNO_3$  99.8 % (PanReac

AppliChem); dehydrated Nutrient Broth (NB), dehydrated Muller Hinton Agar (MHA) and Muller Hinton Broth (MHB) (OXOID); Yeast extract, mycological peptone, and Potato Dextrose Agar (PDA) (HIMEDIA); RPMI-1640 Medium (Sigma) (used as-is). Culture media and other material was sterilized by autoclaving (120 °C, 15 min). Liquid media 1 (M1) was prepared by dissolving NB (13 g  $\cdot$  L $^{-1}$ ) in distilled water. Liquid media 2 (M2) was prepared by dissolving yeast extract (10 g  $\cdot$  L $^{-1}$ ), mycological peptone (10 g  $\cdot$  L $^{-1}$ ) and glucose (20 g  $\cdot$  L $^{-1}$ ) in distilled water. For solid media, agar was added to the respective media (15 g  $\cdot$  L $^{-1}$ ). Pellets resuspensions and dilutions were made using ultrapure sterilized water (Milli-Q).

### 2.2. Microorganisms

### 2.2.1. Microbial cultures for NPs syntheses

Microorganisms were selected based on a literature review of 85 studies published since 2009, referencing 90 microbial strains successfully used for Ag-based NPs synthesis (Sharma et al., 2009; Narayanan and Sakthivel, 2010; Thakkar et al., 2010; Zhang et al., 2016; Singh et al., 2018). Aiming at simplifying purification processes, intracellular syntheses and mold cultures were excluded. We also prioritized mesophilic strains that are reported (Sharma et al., 2009; Narayanan and Sakthivel, 2010; Thakkar et al., 2010; Zhang et al., 2016; Singh et al., 2018) to secrete reductants capable of yielding small, stable AgNPs without harsh capping agents, thereby minimizing both energy input and downstream purification processes. Thus, three bacterial isolates, one strain of Arthrobacter sp. (Ma1) (Dias, 2020) and two Bacillus spp. strains (Bacillus licheniformis - Mb2, and Bacillus sp. - Mu7) (Dias, 2020), together with two yeasts strains, Saccharomyces cerevisiae (Ms5 - Gen-Bank OR790557.1) (Salvador et al., 2023) and Rhodotorula mucilaginosa (Mr6) (Dias, 2020), were selected.

### 2.2.2. Microorganisms for antimicrobial activity assays

Microbial isolates to be tested on antimicrobial activity assays were selected based on their known potential as contaminating agents for CH and had been previously isolated from contaminated cultural heritage materials: *Bacillus cereus* (GenBank OR831969.1) (Dias, 2020; Salvador et al., 2023), *Pseudomonas stutzeri* (Dias, 2020), *Aspergillus niger* (Nunes, 2017), *Penicillium citrinum* (GenBank OR836964.1) (Salvador et al., 2023a), and *Cladosporium ramotenellum* (Dias, 2020).

# 2.3. Ag-based NPs syntheses

Silver-based nanoparticles (Ag-based NPs) were synthesized using cell-free supernatants of microbial cultures (Fig. 1), and all experiments performed in triplicate. Microorganisms were initially grown on solid media and transferred to agar slants for storage (4 °C) until further use. Stock liquid cultures were prepared by inoculating microbial saline suspensions from agar slants (5 mL) into liquid media (95 mL of NB and YB, respectively) and incubated (37 °C, 120 rpm, 24 h for bacteria; 30  $^{\circ}$ C, 120 rpm, 72 h for fungi). Then, for Ag-based NPs synthesis, stock culture (5 mL) was transferred into fresh liquid media (95 mL), incubated under the same conditions, and centrifuged (12000 rpm, 30 min, 4 °C) to remove cells and debris, leaving the supernatants as reaction media. Silver nitrate (1 mm) was added to the supernatants, and the mixtures were incubated (120 rpm, 30 °C, 24 h). Ag-based NPs were isolated and purified by repeated centrifugation (12000 rpm, 60 min, 4 °C) and washed with ultrapure water (2 cycles). The resulting pellets were freeze-dried (24 h), and their mass was determined using a precision scale and the following formula:

$$m_{\textit{pellet}} = m_{(microtube+pellet)} - m_{(microtube)}$$

The pellets were then resuspended in ultrapure water (MilliQ) for a final concentration of 2000 ppm.

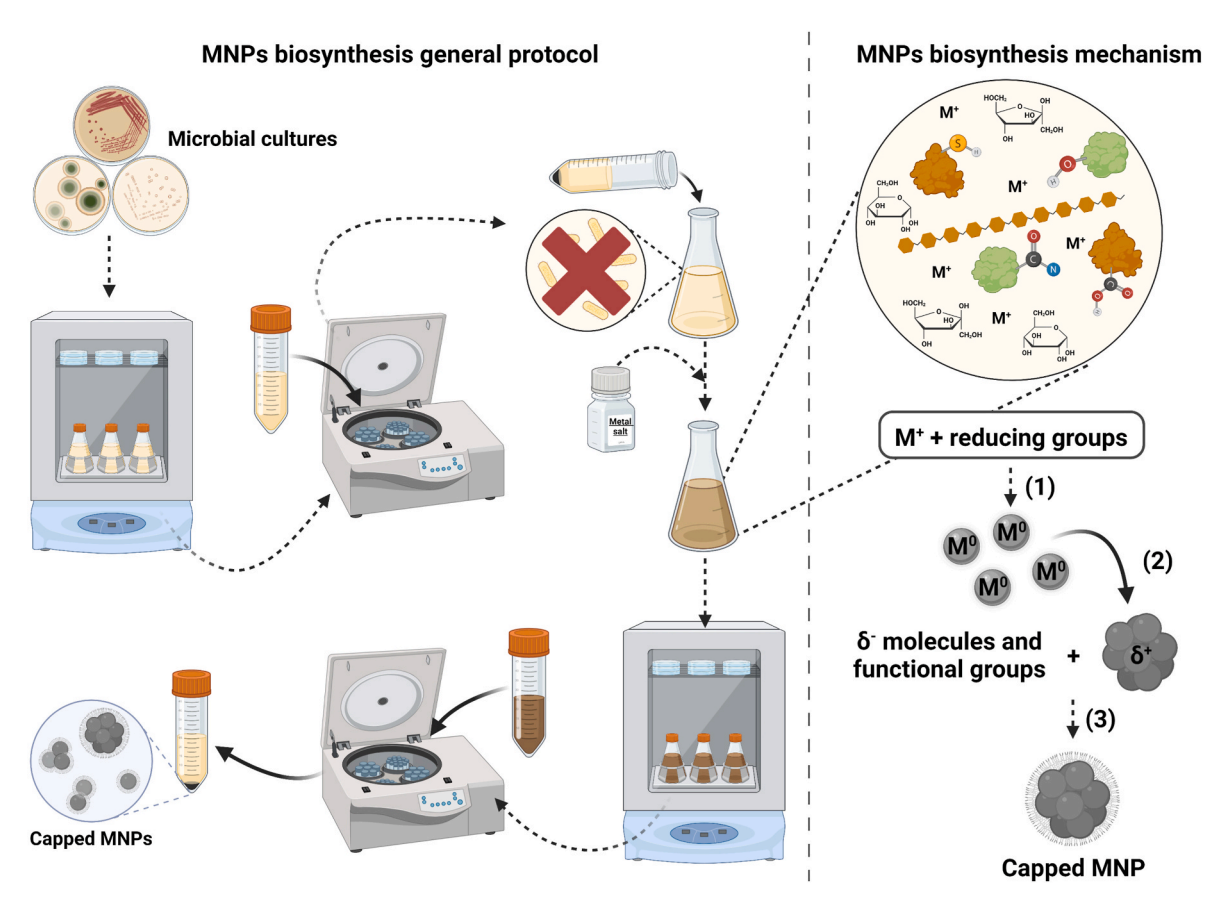


Fig. 1. Protocol for NPs biosynthesis using supernatants of microbial cultures and a simplified hypothetical biosynthesis mechanism. Legend: Reproduced from Carrapico et al., 2023 under creative common CC-BY license.

#### 2.4. NPs characterization

# 2.4.1. Field-emission scanning electron microscopy (FE-SEM)

The morphology (size and shape) of the Ag-based NPs was determined by using FE-SEM (TESCAN CLARA) operating at 20 kV using the backscattered electron detector and the ultra-high-resolution mode. For sample preparation, pellet suspensions were diluted (1:50), placed on top of glass slides (15  $\mu L)$  and dried (1 h, 50 °C). Particle sizes were measured using ImageJ 1.51k software (Schneider et al., 2012).

## 2.4.2. Energy dispersive X-ray spectrometry (EDX)

Elemental mapping and spectra of the Ag-based NPs' suspensions were obtained by using SEM (HITACHI S-3700N) equipped with EDS (BRUKER XFlash 630M) operating at 15 kV (estimated ~20 nA probe current). Spectra of the Ag-based NPs' suspensions used for calibration curve determination were obtained by using UHR FE-SEM (TESCAN CLARA) operating at 20 kV using analysis mode (0.3 nA beam current). Samples were analyzed without dilution on top of glass slides (2  $\mu$ L) after drying (1 h, 50 °C). EDX spectra were analyzed using NIST DTSA-II Oberon (2024-06-11 revision) (Ritchie et al., 2012). Additionally, because the calibration curve was established at 20 kV, whereas most unknowns were measured at 15 kV, we ran Monte Carlo simulations in DTSA-II to quantify how the lower accelerating voltage reduces the Ag X-ray yield and to derive a 15 kV-20 kV correction factor for the net counts. These simulations, performed with the same beam current, consider electron scattering and absorption, allowing cross-voltage comparison of Ag intensities (Ritchie, 2009; Newbury and Ritchie, 2022).

### 2.4.3. X-ray diffraction (XRD)

XRD analysis was performed using a BRUKER D8 Discover X-ray

diffractometer (CuK $\alpha$  radiation ( $\lambda=1.5418$  Å)) to investigate the crystallinity of the synthesized Ag-based NPs. Pellet suspensions (60  $\mu$ L) were placed on top of a Si sample holder, dried (1 h at 50 °C), and then scanned in the 20 range of 5 deg–75 deg at a scan speed of 0.05 deg · s  $^{-1}$ . X-ray diffractograms were analyzed using QualX 2.24 (Altomare et al., 2015) and Profex 5.1.1 (Doebelin and Kleeberg, 2015) software based on the COD (Gražulis et al., 2009; Vaitkus et al., 2021) and RUUFF (Lafuente et al., 2015) databases.

# 2.4.4. Dynamic light scattering (DLS)

Dynamic Light Scattering (DLS) technique was used to obtain the size distribution profile of the synthesized Ag-based NPs in solution. First, solutions were diluted (1:10) using ultrapure water (Milli-Q). Finally, their particle size distribution and dispersity ( $\oplus$ ) were determined by using a particle size analyzer (MALVERN Zetasizer Nano ZS) at 25 °C. Particle sizes were obtained from the average of at least 12 different measurements. Size and  $\oplus$  results' analyses were made using Malvern Zetasizer software v8.02 (Malvern Panalytical, 2021) ("DLS", Supporting information 1).

# 2.4.5. Inductively coupled plasma mass spectrometry (ICP-MS)

The concentration of Ag in the samples was determined using inductively coupled plasma mass spectrometry (ICP-MS) with a triple quadrupole mass spectrometer (Agilent 8800) ("ICP-MS", Supporting information 1). Samples were introduced into the plasma using a pneumatic nebulizer coupled with a spray chamber to ensure consistent aerosol generation (1.01 L  $\cdot$  min<sup>-1</sup> carrier gas flow (Ar); 15 L  $\cdot$  min<sup>-1</sup> plasma gas flow (Ar) rate). To minimize spectral interference, a helium (He) collision cell (4 mL  $\cdot$  min<sup>-1</sup> reaction gas flow) was used, reducing polyatomic interference, particularly from matrix elements. Each sample was measured in triplicate (10 sweeps per replicate). Ag-based NPs

were digested overnight ( $\sim$ 16 h) with nitric acid (65 %, suprapur). After acidic digestion, samples were diluted to a 2 % HNO $_3$  concentration (v/v) with ultrapure water (Milli-Q). Silver quantification was performed by means of an external calibration curve using silver standards solutions prepared in sample-identical matrix conditions. The  $^{107}$ Ag isotope was monitored and used for elemental quantification, and the data processed using a nine-point calibration curve (0, 2, 5, 10, 20, 50, 100, 200, 400 ppb) with a limit of detection (LOD) and limit of quantification (LOQ) of 2.5 ppm and 8.4 ppm, respectively ("ICP-MS", Supporting information 1).

# 2.5. Antimicrobial activity assays

#### 2.5.1. MIC experimental procedures

Minimum Inhibitory Concentration (MIC) assays were adapted from established protocols (Schwalbe et al., 2007; Espinel-Ingroff et al., 2012; Berkow et al., 2020). PDA grown cultures were suspended in a 0.9 % NaCl solution (1.0 x  $10^6$  CFU · mL<sup>-1</sup>) using Neubauer chamber counts. AgNP suspensions were distributed into 96-well microplates and serial dilutions were made in order to obtain concentrations ranging from  $L^{-1}$ , pellet concentration) in each column. Microbial suspensions were added to all rows except one, which contained only sterile Muller Hinton Broth (MHB) as negative controls for microbial growth. This setup vielded six AgNPs concentrations, a positive control (microbial growth) and sterility controls for each replicate. Because each AgNPs suspension was available in limited volume, MIC assays were always run in duplicate where possible and as single replicates when material was insufficient (Table S9, Supporting information 2). Microplates were incubated without agitation at 27  $^{\circ}$ C  $\pm$  2  $^{\circ}$ C for 24 h (*Pseudomonas stutzeri*), 48 h (Arthrobacter sp.), and 72 h (Aspergillus niger and Penicillium citrinum). Because sample volume was limited, the full MIC plus post-exposure regrowth protocol was performed on at least one representative isolate per taxonomic group (Gram-negative, Gram-positive, two filamentous fungi). Bacillus cereus and Cladosporium ramotenellum were assessed only by disc diffusion. After incubation, the plates were examined under a stereoscopic microscope for visible microbial growth (Table S9, Supporting information 2). The MICs were defined as the lowest concentration that completely inhibited visible microbial growth.

## 2.5.2. Post-exposure regrowth assay

Following MIC determination, 10  $\mu$ L from each well showing no visible growth was streaked onto fresh Potato Dextrose Agar (PDA) plates using sterile, disposable calibrated loops, and incubated at 27  $\pm$  2 °C (~24 h for bacteria; ~72 h for fungi) (Schwalbe et al., 2007). Growth of re-inoculated MIC positive controls was used as reference for growth. Plates were read for colony regrowth: absence of colonies indicated bactericidal/fungicidal activity at the tested concentration, whereas visible colonies indicated a bacteriostatic/fungistatic effect. Because our objective was to distinguish lethality qualitatively rather than to document a  $\geq$ 99.9 % CFU reduction, no colony counts were made. The assay therefore yields a qualitative lethality endpoint rather than a formal minimum lethal concentration (MLC).

#### 2.5.3. Disk diffusion assays

Disk diffusion assays were adapted from established methods (Schwalbe et al., 2007; Espinel-Ingroff et al., 2012; Espinel-Ingroff, 2007; Espinel-Ingroff et al., 2011; CLSI, 2014; The European Committee on Antimicrobial Susceptibility Testing, 2023) to evaluate the antimicrobial activity of Ag-based NP suspensions. PDA grown cultures were suspended in a 0.9 % NaCl solution up to  $1.0 \times 10^8$  CFU  $\cdot$  mL $^{-1}$  using Neubauer chamber counts. Microbial suspensions were evenly spread on Mueller-Hinton agar plates (90 mm) with a sterile cotton swab, streaking in three directions to ensure uniform coverage. Then, sterile 6 mm paper filter discs were placed on the plates, and 5  $\mu$ L of AgNPs suspension (2 mg  $\cdot$  mL $^{-1}$  pellet concentration) was applied to each disc. Three

independent plates were prepared for each microbial strain, giving n=3 biological replicates for the disc diffusion assay. Two untreated paper discs served as sterility controls. No commercial antimicrobial disc was included because the objective was to compare AgNPs samples. Inhibition diameters were therefore interpreted relative to the sterile-disc negative control. Plates were then incubated at 27  $^{\circ}\text{C} \pm 2$   $^{\circ}\text{C}$  for 24 h (Pseudomonas stutzeri and Bacillus cereus), 48 h (Aspergillus niger and Penicillium citrinum), or 72 h (Cladosporium ramotenellum). Inhibition zones were measured using ImageJ (Schneider et al., 2012). The disc diameters were averaged from two perpendicular measurements, while inhibition zone diameters were averaged from four straight-line measurements to account for irregular diffusion patterns. The inhibition distance was calculated as:

Inhibition distance = 
$$\frac{Average \ inhibition \ zone \ diameter - Disc \ diameter}{2}$$

This represents the average radial distance from the disc edge to the inhibition zone boundary.

### 2.6. Mathematical models, simulations, and statistical analysis software

### 2.6.1. Mathematical models

Model for EDX quantification of thin films from Ritchie et al. (2023).

$$I_{Film} = \left(rac{\Omega}{4\pi}
ight)\epsilon_{j}\omega_{j}\left(rac{[\imath au]_{\mathrm{Film}}}{q_{e^{-}}}
ight)\left(rac{C_{Z\mathrm{Film}}N}{A_{Z}}
ight)Q_{l}^{Z}(E_{0})FF_{\chi}$$

$$F_{\chi} = \int_{0}^{\infty} \phi_{B}(\rho z) \exp(-\chi_{B} \rho z) d\rho z$$

Ignoring the effects of absorption in the film,  $F_{\chi} = \rho_{Film} \cdot t_{Film}$ ,

$$I_{\mathit{Film}} = \left(rac{arOmega}{4\pi}
ight) \epsilon_j \omega_j \left(rac{[\imath au]_{\mathrm{Film}}}{q_{e^-}}
ight) \left(rac{C_{\mathit{ZFilm}} N}{A_Z}
ight) Q_l^Z(E_0) F 
ho_{\mathit{Film}} t_{\mathit{Film}}$$

Where:

 $I_{Film}$  – characteristic X-ray intensity for the j-th transition (net counts)

 $\Omega$  – detector solid angle (sr)

 $\pi$  – number pi

 $\epsilon_j$  – fractional detector efficiency for j-line (this term cancels)

 $\omega_i$  – fluorescence yield (dimentionless)

 $[\iota\tau]_{\text{Film}}$  – probe dose (nA · s)

 $q_{e^-}$  – electron charge (C)

 $C_{ZFilm}$  – mass fraction of element Z (g · g<sup>-1</sup>)

N – Avogadro's Number (mol<sup>-1</sup>)

 $A_Z$  – atomic weight of the Ag (g)

 $Q_l^Z(E_0)$  – ionization cross-section for the l-shell of Ag for electrons of kinetic energy  $E_0$ . (cm<sup>2</sup>)

*F* – secondary fluorescence correction (dimentionless)

 $\rho_{Film}$  – density of the film constituent material (g  $\cdot$  cm<sup>-3</sup>)

 $t_{Film}$  – film thickness (cm)

Simplifying:

 $I_{\mathrm{Film}} = k_{1,Ag} k_{2,keV} \cdot [\iota \tau]_{\mathrm{Film}} \cdot \rho_{\mathit{Film}} \cdot t_{\mathit{Film}}$ 

Since  $\rho_{Film} \cdot t_{Film} = \frac{m_{Ag}}{S}$ ,

$$I_{\mathrm{Film}} = k_{1,Ag} k_{2,keV} [\iota \tau]_{\mathrm{Film}} \frac{m_{Ag}}{S}$$

 $k_{1,Ag}$  – constant terms dependent of Ag properties

 $k_{2,keV}$  – constant terms dependent of incident beam energy (E<sub>0</sub>)

 $m_{Ag}$  – total mass of Ag (g)

S – area of analysis (cm<sup>2</sup>)

Model for silver ions release from nanoparticles developed from the Arrhenius equation from Zhan et al. (Zhang et al., 2011).

$$\gamma_{Ag^{+}} = \frac{3}{4} \left( \frac{8\pi k_{B}T}{m_{B}} \right)^{1/2} \rho^{-1} e^{\left( \frac{-E_{a}}{k_{B}T} \right)} [Ag] r^{-1} [O_{2}]^{1/2} [H^{+}]^{2}$$

Where:

 $\gamma_{Ag^+}$  – release rate of Ag<sup>+</sup> form NPs (mol · L<sup>-1</sup> · h<sup>-1</sup>)  $\pi$  – number pi

 $k_{\rm B}$  – Boltzmann's constant (J · K<sup>-1</sup>)

T – Temperature (K)

 $m_B$  – molar mass of Ag (g · mol<sup>-1</sup>)

 $\rho$  – density of particles (g · cm<sup>-3</sup>)

 $E_a$  – activation energy for Ag oxidation (J)

[Ag] - total concentration of silver (mol  $\cdot$  L<sup>-1</sup>)

r – NPs' radius (nm)

 $[O_2]^{1/2}$  – concentration of dissolved  $O_2$  (mol · L<sup>-1</sup>)

 $[H^+]^2$  – concentration of H<sup>+</sup> in solution (mol · L<sup>-1</sup>)

Assuming T,  $[O_2]^{1/2}$ ,  $[H^+]^2$  constants, then:

$$\gamma_{Ag^+} = \kappa_{3,Ag}[Ag]r^{-1}\rho^{-1}$$

Where:

$$\kappa_{3,Ag} = \frac{3}{4} \left( \frac{8\pi k_B T}{m_B} \right)^{1/2} e^{\left( \frac{-E_a}{k_B T} \right)} [O_2]^{1/2} [H^+]^2$$

Normalizing for  $r^{-1}\rho^{-1}$  by multiplying both terms by these parameters gives:

$$\gamma_{Ag^+} \cdot r \cdot \rho \propto \kappa_{3,Ag}[Ag]$$

#### 2.6.2. Simulations and statistical analysis software

Monte Carlo simulations for EDX quantification corrections were made using NIST-DTSAII (Ritchie, 2009; Ritchie et al., 2023). Statistical analyses and graphics were made using R Studio (Posit team, 2024).

#### 3. Results and discussion

### 3.1. Characterization of biosynthesized NPs

# 3.1.1. Quantification of Ag

An approach using both ICP-MS and EDX analysis was used for quantification of silver in samples containing AgNPs. These samples were used as in-house standards. They were digested in HNO<sub>3</sub> 65 %, diluted to HNO<sub>3</sub> 2 % (after digestion), and quantified for <sup>107</sup>Ag using ICP-MS. These same samples were also analyzed using EDX. Based on the model for quantification of thin films  $\left(I_{\text{Film}} = k_{1,Ag} k_{2,keV} [\iota \tau]_{\text{Film}} \frac{m_{Ag}}{S}\right)$ , Ag net counts obtained from EDX analysis were multiplied by the area of acquisition (cm<sup>2</sup>) and divided by the probe dose (nA  $\cdot$  s) which resulted in a normalized intensity measurement  $I_{Ag,norm}$  (cm<sup>2</sup> · nA<sup>-1</sup> · s<sup>-1</sup>).  $I_{Ag,norm}$ norm values were then plotted against the Ag<sub>mass</sub> (μg) obtained from ICP-MS (Fig. 2) ("EDX|ICP-MS quantification", Supporting information 1), which showed a good linear correlation, therefore enabling the determination of  $Ag_{mass}$  from Ag net counts obtained by EDX analysis ( $E_0 =$ 20 kV).

ICP-MS quantification for biosynthesized NPs was not possible due to equipment and sample unavailability. However, they were analyzed using EDX. Therefore, to estimate the Ag<sub>mass</sub>, the correlation between IAg,norm and Agmass from EDX analysis could be applied. However, since the experimental accelerating voltage (E<sub>0</sub>) used was 15 kV, the model

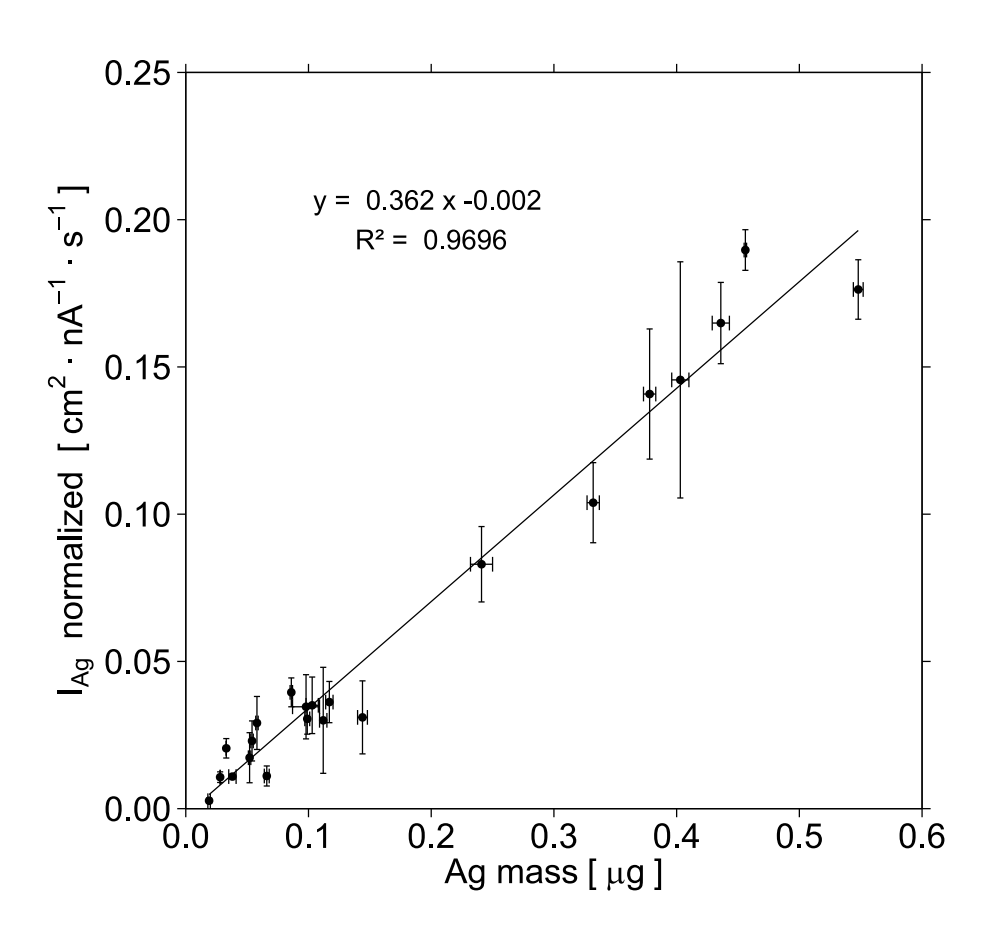


Fig. 2. Calibration curve for determining silver mass ( $\mu g$ ) from normalized EDX intensity ( $I_{Ag,norm}$ ).

developed for 20 kV could not be directly applied. To address this, Monte Carlo simulations were performed using NIST DTSAII (Newbury and Ritchie, 2022; Ritchie et al., 2023) to correct EDX counts from 15 kV to 20 kV (Tables S5 and S6, Supporting information 2). First, the experimental analytical conditions and parameters were added into the software, and simulations were run to generate EDX spectra. These simulated spectra were compared with experimental spectra to validate the accuracy of the simulations. Next, with all other parameters held constant,  $E_0$  was adjusted to 20 kV, and new simulations were run.

Finally, the ratio of signal intensities for Ag at 15 kV and 20 kV  $\left(\frac{I_{Ag.15~kV}}{I_{Ag.20~kV}}\right)$ 

was calculated and used to correct experimental data.

The corrected Ag net count from the biosynthesized NPs samples were normalized by applying the rational presented above for the calibration curve samples, based on the model for EDX analysis of thin films (Ritchie et al., 2023). This resulted in  $I_{Ag,norm}$  values for the samples, which were then used to determine the mass and concentration of Ag, applying the calibration curve formula (Table 1) ("EDX|ICP-MS quantification", Supporting information 1).

#### 3.1.2. Morphology

Nanoparticle size and morphology were analyzed using field emission scanning electron microscopy (FE-SEM) and dynamic light scattering (DLS). SEM allows direct observation of nanoparticle morphology and individual sizes, whereas DLS provides size distributions of nanoparticles in colloidal form. Given that the particles ranged from 15 to 67 nm, the resolution provided by FE-SEM (~1.5 nm) (Bhattacharya and Acharya, 2020) was sufficient for accurate size measurement. FE-SEM images confirmed the production of predominantly spheroid nanoparticles within the size range of 1-100 nm (Table 2) (Fig. S1 and Tables S1, S2, and S3, Supporting information 2; "SEM analysis", Supporting information 1). DLS results show larger hydrodynamic diameters compared to direct size measurements from SEM, which is consistent with the influence of solvation layers and the sensitivity of the Z-average to larger particles within the distribution. The dispersity (Đ) values indicate variability in particle sizes, suggesting a degree of heterogeneity in the samples' aggregation in suspension (Table 2; "DLS", Supporting information 1). The combined results from FE-SEM and DLS confirm the successful biosynthesis of nanoparticles using supernatants of microbial cultures, with predominantly spherical morphology and a size range within the nanoscale.

## 3.1.3. Elemental and molecular analysis

Energy-dispersive X-ray spectrometry (EDX) was employed to

**Table 1**Silver concentration of biosynthesized NPs determined via ICP-MS, EDX, thin-film models, and Monte-Carlo simulations.

Sample	$I_{corrected,Ag} \; [cm^2 \cdot nA^{-1} \cdot \; s^{-1}]^{a)}$	$Ag_{mass}\left[\mu g\right]^{b)}$	Ag <sub>concentration</sub> [ppm] <sup>c)</sup>
M1	0.479	1.30	650
M1Ma1	0.443	1.20	600
M1Mb2	0.511	1.38	692
M1Ms5	1.278	3.46	1729
M1Mr6	0.849	2.30	1149
M1Mu7	0.606	1.64	821
M2	0.005	0.02	10
M2Ma1	0.082	0.23	113
M2Mb2	0.258	0.70	351
M2Ms5	0.284	0.77	386
M2Mr6	0.139	0.38	190
M2Mu7	0.139	0.38	190

 $<sup>^{\</sup>rm a)}$   $I_{\rm corrected,Ag}$  was obtained by applying the model for EDX analysis of thin films (Ritchie et al., 2023), after correction for  $E_0$  using Monte Carlo simulations (Newbury and Ritchie, 2022).

 $\begin{tabular}{ll} \textbf{Table 2} \\ \textbf{Size and hydrodynamic properties of biosynthesized NPs from SEM and DLS} \\ \textbf{analyses.} \\ \end{tabular}$ 

Sample	SEM [nm] <sup>a)</sup>	Z-Average [nm] <sup>b)</sup>	$\mathbf{\tilde{D}^{c)}}$
M1	$22\pm 5$	208	0.442
M1Ma1	$15\pm3$	76	0.203
M1Mb2	$37\pm18$	152	0.341
M1Ms5	d	110	0.559
M1Mr6	$67 \pm 24$	115	0.082
M1Mu7	d	85	0.302
M2	d	168	0.360
M2Ma1	$17\pm3$	138	0.165
M2Mb2	$20 \pm 4$	50	0.458
M2Ms5	$16 \pm 3$	100	0.184
M2Mr6	$32\pm16$	112	0.356
M1Mu7	d	81	0.392

<sup>&</sup>lt;sup>a)</sup> SEM sizes determined from the average of ≥50 individual NPs measurements of FE-SEM-UHR images, using ImageJ software.

analyze the elemental composition of the nanoparticles and to preliminary identify potential interactions or compound formations. EDX mapping provided insights into the spatial distribution of elements, while semi-quantitative analysis was used to estimate atomic ratios of key elements, such as Ag and Cl (Table 3) (Table S4, Supporting information 2). For nanoparticles synthesized using YB, EDX detected the presence of Ag as the primary element, accompanied by vestigial concentrations of C, S, and P ("EDX semi-quantification", Supporting information 1). These elements are likely associated with the nanoparticles' protein corona, which forms due to the adsorption of biomolecules on the nanoparticle surface during biosynthesis (Monopoli et al., 2011). While most samples were well purified, a subset showed residual impurities, as suggested by diffuse features in FE-SEM images. These samples underwent an additional purification cycle to ensure consistent quality prior to antimicrobial testing. In samples synthesized using NB, a similar elemental profile was observed, with the inclusion of Cl. Semi-quantitative EDX analysis revealed Ag:Cl atomic ratios close to 1:1, and mapping showed significant overlap between Ag and Cl signals (Table S4, Supporting information 2; "EDX semi-quantification", Supporting information 1). These results suggest the formation of AgCl nanoparticles (AgClNPs) alongside AgNPs, depending on the initial reaction conditions.

XRD analysis confirmed the molecular composition and crystalline structure of the biosynthesized nanoparticles (Table 3; Table S7,

 Table 3

 Elemental composition and crystalline structures of biosynthesized NPs.

Sample	Ag:Cl <sub>atom</sub> (EDX) <sup>a)</sup>	Crystalline structure (XRD)
M1	0.8	Chlorargyrite (fccc, AgCl)
M1Ma1	1.3	Chlorargyrite (fccc, AgCl)
M1Mb2	1.2	Chlorargyrite (fccc, AgCl)
M1Ms5	1.0	Chlorargyrite (fccc, AgCl)
M1Mr6	1.0	Chlorargyrite (fccc, AgCl)
M1Mu7	1.2	Chlorargyrite (fccc, AgCl)
M2	d	Chlorargyrite (fccc, AgCl)
M2Ma1	5.0	Amorphous
M2Mb2	9.0	Amorphous
M2Ms5	Ag only <sup>b)</sup>	Silver (fcc <sup>c)</sup> , Ag)
M2Mr6	Ag only <sup>b)</sup>	Silver (fcc <sup>c)</sup> , Ag)
M1Mu7	Ag only <sup>b)</sup>	e

a) Ag:Cl<sub>atom</sub>: Ag:Cl atomic ratio from EDX after correction for background.

 $<sup>^{\</sup>rm b)}$  Ag<sub>mass</sub> was obtained from the calibration curve of I<sub>corrected,Ag</sub> from EDX vs. Ag<sub>mass</sub> from ICP-MS quantification, assuming continuous linearity.

 $<sup>^{\</sup>tilde{c})}$  Ag\_{concentration} was calculated using the analysis volume of 2  $\mu L$ 

b) Z-Average: average hydrodynamic diameter of the NPs suspended in ultrapure water (MilliO).

c) D: dispersity. DLS results analyzed using Zetasizer software v8.02.

d) Not possible to acquire good resolution FE-SEM images.

b) Ag only: vestigial or no Cl was detected.

c) fcc: face cubic centered crystalline structure.

d) Not possible to determine ratio.

e) Not possible to obtain diffractogram.

Supporting information 2), complementing EDX results. Diffractograms of NB-synthesized samples revealed sharp, well-defined peaks associated with AgClNPs, exhibiting face-centered cubic (fcc) crystalline structures. Characteristic peaks from planes (111), (200), (220), and (311) confirmed the formation of chlorargyrite (AgCl). In contrast, YBsynthesized samples exhibited broader peaks, due to their lower concentrations, and amorphous bands, revealing the presence of noncrystalline material. M2Ms5 and M2Mr6 exhibited fcc crystalline peaks corresponding to silver planes (111) and (200). For samples M2Ma1 and M2Mb2, the lack of detectable Cl, despite the observed amorphous patterns, suggests the presence of non-crystalline AgNPs. For sample M2, vestigial peaks from planes (111), (200), (220), and (311) suggest the formation of chlorargyrite (AgCl). This conflicts with the EDX analysis of M2, where only silver was detected. A possible explanation for this discrepancy is the low concentration of sample M2, which, under the conditions used for EDX analysis might not allow for Cl detection. Additionally, XRD was performed on a film produced by evaporating 60 µL of suspension, therefore the diffractometer analyzed a relatively large and thick film in which even a minor crystalline AgCl fraction could be detected. EDX, by contrast, analyzed a much smaller and thinner film obtained from only 2 µL which could make Cl signal undetectable. Together, the smaller sampling volume and surfaceweighted nature of EDX may account for the absence of Cl in EDX despite the AgCl vestigial signature in XRD. The differences between M2 (AgClNPs) and the remaining YB-synthesized samples (AgNPs), while needing further research, hint for the influence of the microorganisms in the concentration of Cl<sup>-</sup> which changes the NPs composition. Overall, XRD and EDX analyses suggest that NB conditions favor the formation of crystalline AgClNPs, while YB conditions result in a mixture of crystalline and amorphous AgNPs, with compositions influenced by reaction medium properties and microorganisms, as expected.

#### 3.2. Antimicrobial activity

After characterization, all nanoparticle suspensions were screened against microorganisms isolated from contaminated cultural-heritage

materials. Antimicrobial activity was evaluated by minimum inhibitory concentration (MIC) assays, post-exposure regrowth assays and disc-diffusion tests. Because each pellet was standardized to 2 mg mL $^{-1}$ , the remaining volume was limited; as a result, some suspensions could not be assessed by every method, and the MIC dilution series could not be extended below 3–27 ppm (lower bound determined by the initial sample concentration). MIC values that coincided with this lowest concentration are flagged in the Fig. 3 and "MIC", Supporting Information 1, to indicate that the true MIC may be lower.

### 3.2.1. Broth microdilution assays

The antimicrobial potential of NPs was analyzed using broth microdilution assays to determine minimum inhibitory concentrations (MICs). These assays provide quantitative insights into the lowest concentration of NPs required to inhibit microbial growth. MIC values were determined against two bacterial strains (*Arthrobacter* sp. and *Pseudomonas stutzeri*), and two fungal strains (*Aspergillus niger* and *Penicillium citrinum*) isolated from contaminated cultural heritage materials. Most NP suspensions demonstrated low MIC values, ranging from 3 to 28 ppm, with a few exceptions. Notably, for several suspensions the MIC corresponded to the lowest concentration tested, suggesting that the true MIC could be even lower (Fig. 3). Because sample volume was limited, we could not repeat the assay to extend the dilution series below the 3–27 ppm range available for each batch. In future approaches biosynthesis will be scaled up so that a more exhaustive dilution series can be performed.

These results highlight the high antimicrobial potential of the bio-synthesized NPs and are in line with observations from other studies where the antimicrobial concentration range is similar between gramnegative and gram-positive bacteria and between eukaryotic and prokaryotic cells (Greulich et al., 2012; Loza et al., 2014a). Table 4 summarizes seven examples of recent studies covering biosynthesized, chemically, physically and commercially produced silver nanoparticles. The AgNPs biosynthesized in this study (MIC 3–28 ppm) fall at the low end of the reported range. Their performance is comparable to other green preparations such as those resulting from fruit extracts (2.1–21

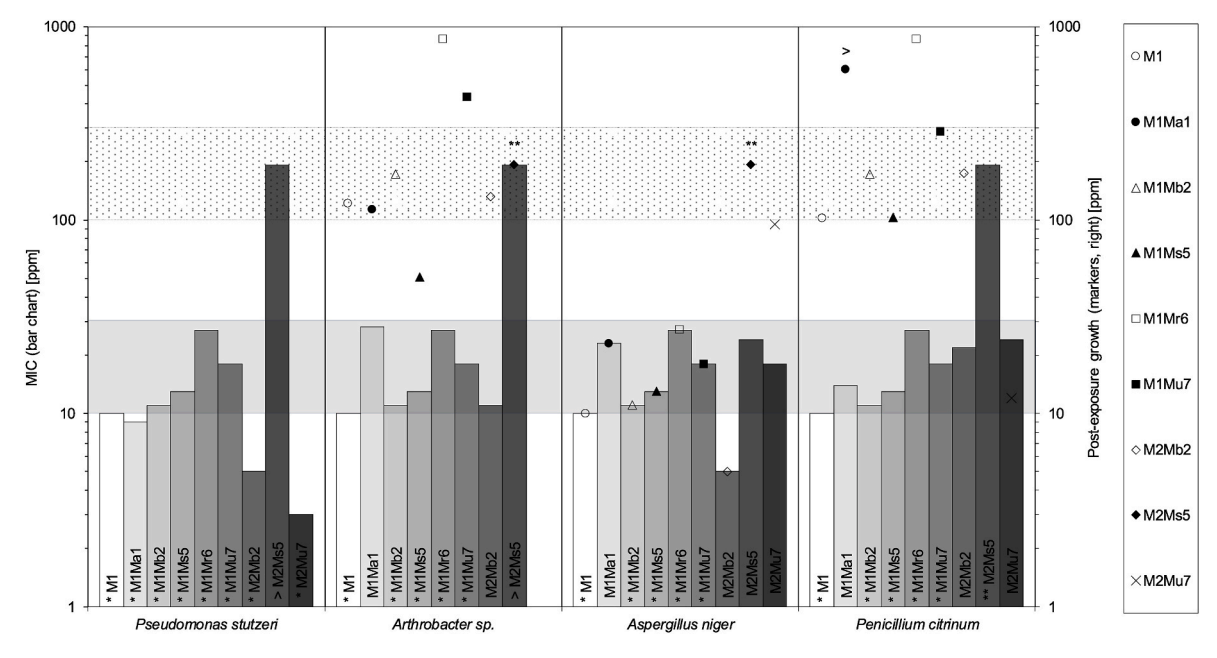


Fig. 3. MIC and post-exposure regrowth results for nine nanoparticle suspensions against microbial isolates of cultural heritage.

Legend: Bar charts: minimum inhibitory concentration (MIC); Markers: post-exposure regrowth; The shaded area highlights the range where most MIC values fall (10–30 ppm), and the dotted area indicates the range where most post-growth inhibitory values fall (100–300 ppm). \*Lowest ppm tested; \*\*highest ppm tested; ">" indicates values exceeding the highest ppm tested. MIC values for M1, M1Ma1, M1r6, and M2Mb2 were calculated as the average of two replicates. MIC values for M1Mb2, M1Ms5, and M2Ms5 were derived from single replicates. Results for M2Mu7 against Arthrobacter sp. were invalid. Results for Pseudomonas stutzeri were discarded as no growth was observed after inoculation.

**Table 4**Comparative examples of MIC intervals of AgNPs synthesized by different routes.

Syntheses	Size (nm) <sup>a</sup>	Capping	Tested cultures	MIC (ppm)	Ref.
Biological					
Microbial supernatants	15-60	Protein corona <sup>b</sup>	Arthrobacter sp.;	3-28	This study
			Pseudomonas stutzeri; A. niger; Penicillium citrinum		
Microbial supernatants (kefir)	50-200	Protein corona <sup>b</sup>	A. baumannii;	25-50	Bernardes et al. (2025)
			K. pneumoniae		
Plant-extract (guarana)	40–49	Phenolic compounds	E. coli; S. aureus;	2.1-21	Lima et al. (2024)
			A. fumigatus;		
			P. chrysogenum;		
			F. oxysporum;		
		b	C. albicans		
Plant-extract (banana and orange)	53–56	Protein corona <sup>b</sup>	B. cereus; S. aureus;	3.1-12.5	Kifle et al. (2025)
			E. coli; M. morganii;		
			A. niger; P. digitatum;		
			A. alternata;		
Chemical			F. oxysporum		
Polyol method (spheres)	35–50	PVP	ESKAPE panel	12.5–25	Holubnycha et al. (2024)
Photomediated (cubes)	45–75	PVP	ESKAPE panel	2.5–5	Holubnycha et al. (2024)
Borohydride-citrate reduction	~11 <sup>c</sup>	Citrate	Pseudomonas spp.	2.6-21.3	Kamer et al. (2024)
Physical					
Laser ablation	~83 <sup>c</sup>	Ligand-free	E. coli; S. aureus	5.4-37.8	Morone et al. (2024)
Arc-discharge	~20 <sup>c</sup>	Carbon shell	P. aeruginosa strains	2–16	Elwakil et al. (2024)
Commercial (Spray pyrolysis <sup>b</sup> )	15-25	Ligand-free <sup>b</sup>	E. coli;	16-256	Alotaibi et al. (2022)
			K. pneumoniae;		
			P. aeruginosa;		
			A. baumani; Staphylococcus spp.		

<sup>&</sup>lt;sup>a</sup> Size reported from electron microscopy image measurements (SEM or TEM).

ppm and 3.1-12.5 ppm) (Lima et al., 2024; Kifle et al., 2025) and superior to other microbial supernatants particles (25–50 ppm) (Bernardes et al., 2025). Chemically synthesized particles show similar intervals polyol-PVP spheres require 12.5-25 ppm (Holubnycha et al., 2024) and borohydride-citrate AgNPs 2.6-21.25 ppm (Kamer et al., 2024) whereas nanocubes achieve lower MICs at 2.5-5 ppm (Holubnycha et al., 2024). Among physically produced AgNPs, ligand-free arc-discharge (2-16 ppm) (Elwakil et al., 2024) and laser ablated (5.4-37.8 ppm) (Morone et al., 2024) AgNPs approach or equal the MIC values from this study, but both rely on energy-intensive apparatus and lack the biogenic surface corona that improves colloidal stability and may reduce cytotoxicity. Reported commercial AgNPs inhibited Gram-negative bacteria at 16-128 ppm and Gram-positives up to 256 ppm (Alotaibi et al., 2022). Taken together, these comparisons indicate that this work's microbial supernatant route results in silver nanoparticles whose antimicrobial efficacy equals or exceeds that of other laboratory and commercial formulations, while avoiding toxic reductants, high temperatures and specialized equipment - features that favor cultural heritage conservation with reduced energy consumption, toxic wastes and

The variability in MIC values among different NP suspensions may be attributed to several factors (e.g., differences in particle size, silver ion release rates, and interactions with microbial cell walls). However, due to the variable concentrations tested, values could not be tested for any dependence. Nevertheless, we could still observe small differences between microorganisms which suggest that their individual structural and metabolic features influence susceptibility to NPs, while remaining in the same concentration range.

Additionally, a strong inverse relationship between dispersity (Đ) and MIC was observed, whereas hydrodynamic size (Z-average) showed no clear relationship. Because DLS is intensity-weighted (scattering  $\alpha$  d $^6$ ), large particle or aggregates inflate both size and dispersity measurements, effectively masking any minority fraction of smaller particles. SEM images confirmed that the "high dispersity" suspensions still contain many (mostly) small particles (Table 2) (Fig. S1 and Tables S1, S2, and S3, Supporting information 2; "SEM analysis", Supporting

information 1). When dispersity is considered – i.e., Z-average standard deviation and SEM sizes are equated – smaller sizes tend to coincide with stronger antimicrobial activity (lower MICs), in agreement with the literature (Menichetti et al., 2023; Ali et al., 2024). Thus, the dispersity correlation is indirect: heterogeneity matters only insofar as it signals the coexistence of a population of smaller particles that likely govern antimicrobial potency in liquid media through their higher surface-area-to-volume ratio, faster  $\mathrm{Ag}^+$  release, and easier cell uptake, whereas larger particles lack these advantages.

#### 3.2.2. Post-exposure regrowth

To distinguish between bacteriostatic/fungistatic and bactericidal/ fungicidal activity, 10 µL of samples from the broth microdilution assays that showed no visible microbial growth (> MIC value) were transferred onto fresh PDA plates (free of nanoparticles) using sterilized and calibrated plastic loops. This assay enabled the distinction between staticonly activity and lethality and allowed for the comparison of effects at different concentrations. Most NP suspensions demonstrated lethal activity, but generally at significantly higher concentrations than those required for growth inhibition (Fig. 3). For example, while almost all MIC values observed were between 10 and 30 ppm (Fig. 3, shaded area), regrowth was completely inhibited only at much higher concentrations (~10-fold increase), mostly between 100 and 300 ppm (Fig. 3, dotted area), with the clear exception of Aspergillus niger, whose lethal concentrations are marginally higher than their MICs. These differences between MIC and post-exposure growth suggest that at low NP concentrations microbial growth is inhibited by reversible mechanisms that are not related with cell death while at higher concentrations these mechanisms do activate.

These findings support the importance of distinguishing between growth inhibition and lethal effects when assessing nanoparticle antimicrobial activity, particularly when balancing between desired effect and potential toxicity. They also highlight the high antimicrobial potential of the biosynthesized NPs, as evidenced by their low MIC values and their ability to achieve lethal effects at higher concentrations against CH contaminating microorganisms.

<sup>&</sup>lt;sup>b</sup> Probable/hypothesized/inferred.

<sup>&</sup>lt;sup>c</sup> Average size.

#### 3.2.3. Disk diffusion assays

NPs antimicrobial potential was also studied on MHA plates against microorganisms isolated from contaminated cultural heritage materials, using disc diffusion assays. After incubation we used image analysis software ImageJ to precisely measure the inhibition zone diameter. (Table 5) (Table 8, Supporting information 2; "Disc diffusion analysis", Supporting information 1).

Generally, at lower silver concentrations (<500 ppm), little or no inhibition was observed, while a sharp increase occurred between 500 and 1000 ppm. Beyond 1000 ppm, inhibition zones plateaued, revealing that further increases in silver concentration did not enhance inhibition (Fig. 4). We hypothesized that this plateau effect could reflect the result from a balance between the growth rate of microorganisms and the diffusion rate of Ag-based NPs through the agar medium.

Since this plateau at higher concentrations was unexpected, we decided to investigate the profiles for different microbial cultures individually. Inhibition data across all tested strains (Fig. 5) ("Disc diffusion analysis", Supporting information 1), showed a consistent pattern: a lag phase with no inhibition at low concentrations, a linear relationship (variable between microorganisms) at intermediate concentrations, and the plateau at higher concentrations. Slower-growing microorganisms, such as the filamentous fungi *P. citrinum* and *A. niger*, showed greater inhibition zones at higher silver concentrations compared to faster-growing bacteria, such as *P. stutzeri* and *B. cereus*. This observation suggested that slower growth rates allow fungi to experience greater inhibitory effects due to the extended time available for Ag-based NPs to diffuse through the agar medium. In contrast, bacteria establish colonies more quickly, potentially outpacing the diffusion of silver ions and resulting in smaller inhibition zones.

Nevertheless, this trend did not apply universally. Cladosporium ramotenellum, the slowest-growing microorganism tested, displayed inhibition patterns similar to bacterial isolates (Fig. 5), suggesting that susceptibility differences were not solely attributable to microbial growth rates or metabolic distinctions between fungi and bacteria. Instead, the balance between growth rate and nanoparticle diffusion appeared to be the key factor. For slower-growing microorganisms, diffusion has more time to establish effective concentration gradients, resulting in larger inhibition zones. However, in the case of C. ramotenellum, the prolonged diffusion time may lead to a "dilution effect," where silver ions are distributed over a larger area, reducing local concentrations by the time microbial growth begins.

At lower concentrations Ag-based NPs primarily exhibit microbiostatic rather than microbiocidal activity, as observed from MIC and post-exposure assays comparison. If microorganisms grow rapidly before the nanoparticles diffuse sufficiently, their growth may not be effectively inhibited, leading to smaller inhibition zones.

#### 3.2.4. Disc diffusion kinetics

Studies have shown a clear relationship between agar concentration in culture media and pore size, which directly impacts nanoparticle (NP) diffusion (Ackers and Steere, 1962; Pluen et al., 1999). At commonly used agar concentrations (~1.5 % w/v), the average pore size is approximately 100 nm (Ackers and Steere, 1962). According to the Stokes-Einstein relation, the free diffusion rate of particles in solution is inversely proportional to their hydrodynamic radius (Stokes, 1851; Einstein, 1905). However, in agar gels, diffusion is further restricted by the particle-to-pore size ratio, with the restriction following an exponential decay relationship (Ackers and Steere, 1962). This means that as the particle size approaches the pore size, diffusion becomes increasingly difficult. For nanoparticles with a hydrodynamic radius of 40 nm or larger (a/r > 0.5), over 90 % diffusion restriction is expected in 1.5 % agar gels (Ackers and Steere, 1962). These findings suggest that antimicrobial activity observed in disc diffusion assays is unlikely driven by direct nanoparticle diffusion. Therefore, other mechanisms, such as the dissolution rate of silver ions from NPs must be considered, which may lead to a critical distinction at interpreting assay results.

Published studies have suggested that the antimicrobial activity observed in disc diffusion assays with metal nanoparticles (NPs) is primarily due to silver ion release rather than direct NP diffusion (Kourmouli et al., 2018; Loza et al., 2014a). These studies have also raised concerns about the validity of conclusions drawn from such assays, particularly regarding their applicability to evaluating nanoparticle efficacy (Gopal et al., 2018; Kourmouli et al., 2018; Loza et al., 2014b). However, direct empirical evidence linking silver ion release to the inhibition observed in disc diffusion assays has been lacking.

Zhan et al. developed and validated a model for silver ion release from nanoparticles based on the Arrhenius equation (Zhang et al., 2011):

$$\gamma_{Ag^+} = rac{3}{4} \left(rac{8\pi k_B T}{m_B}
ight)^{1/2} 
ho^{-1} e^{\left(rac{-E_g}{k_B T}
ight)} [Ag] r^{-1} [O_2]^{1/2} [H^+]^2$$

Has previously shown (Fig. 4b), we also identified a good Arrhenius-like correlation between silver concentration and microbial inhibition. This led us to test, for the first time using empirical data, whether the inhibition observed in disc diffusion assays is directly linked to silver ion release from the nanoparticles rather than NP diffusion. Our approach was as follows: assuming that all parameters in the model except for particle radius (r) and density ( $\rho$ ) remain constant, the silver release rate ( $\gamma_{Ag^+}$ ) should scale proportionally with the initial silver concentration (Ag<sub>concentration</sub>) divided by the NP radius and density. By normalizing the silver concentration and microbial inhibition data by these factors, we derived the following proportional relationship:

$$\gamma_{Ag^+} \cdot r \cdot \rho \propto \kappa_{3,Ag}[Ag]$$

**Table 5**Inhibition from disc diffusion assays of biosynthesized NPs against microorganisms isolated from cultural heritage materials.

NPs samples	Inhibition distance from	Inhibition distance from disc hedge (mm) <sup>a)</sup>							
	Pseudomonas stutzeri	Bacillus cereus	Aspergillus niger	Penicillium citrinum	Cladosporium ramotenellum	Average <sup>b)</sup>			
M1	$0.69 \pm 0.27$	$0.73\pm0.03$	$0.49\pm0.25$	$1.55\pm0.41$	$0.80 \pm 0.07$	$0.81\pm0.10$			
M1Ma1	$0.12\pm0.13$	$0.34 \pm 0.05$	$0.92\pm0.85$	$1.22\pm0.28$	$0.76\pm0.17$	$0.63\pm0.09$			
M1Mb2	$0.53\pm0.13$	$0.76\pm0.18$	$0.34 \pm 0.06$	$1.34\pm0.44$	$0.87\pm0.11$	$0.42\pm0.87$			
M1Ms5	$1.35\pm0.20$	$0.94 \pm 0.03$	$2.03\pm0.23$	$2.57\pm0.19$	$1.33\pm0.30$	$1.64\pm0.15$			
M1Mr6	$1.03\pm0.29$	$1.24 \pm 0.10$	$1.66\pm0.27$	$2.30\pm0.14$	$1.26\pm0.12$	$1.50\pm0.12$			
M1Mu7	$0.42\pm0.08$	$0.55\pm0.19$	$0.98\pm0.13$	$1.07\pm0.20$	$1.54\pm0.32$	$0.92\pm0.10$			
M2	n.i.	n.i.	n.i.	n.i.	n.i.	n.i.			
M2Ma1	n.i.	n.i.	n.i.	n.i.	n.i.	n.i.			
M2Mb2	$0.08\pm0.07$	n.i.	n.i.	n.i.	n.i.	$0.04\pm0.02$			
M2Ms5	n.i.	n.i.	n.i.	n.i.	n.i.	n.i.			
M2Mr6	n.i.	n.i.	n.i.	n.i.	n.i.	n.i.			
M2Mu7	n.i.	n.i.	n.i.	n.i.	n.i.	n.i.			

 $<sup>\</sup>frac{a}{b}$  Values represent the average inhibition distance, in mm, from the edge of the disc to the onset of culture growth (averages of triplicates  $\pm$  standard deviation).

b) The "Average" column refers to the average inhibition distance across the four microorganisms tested. n.i.: no measurable inhibition – corresponding to 0.00 mm.

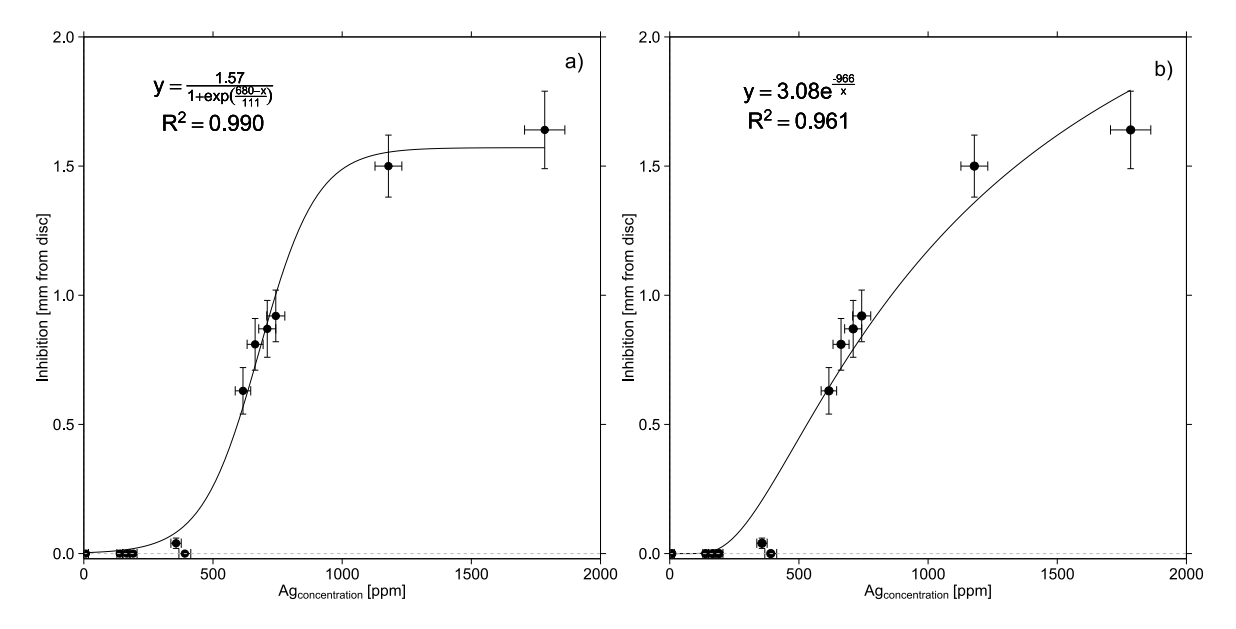


**Fig. 4.** Inhibition vs. Ag concentration curve fitting profiles. Legend: a) Sigmoidal curve fitting. b) Arrhenius-like curve fitting.

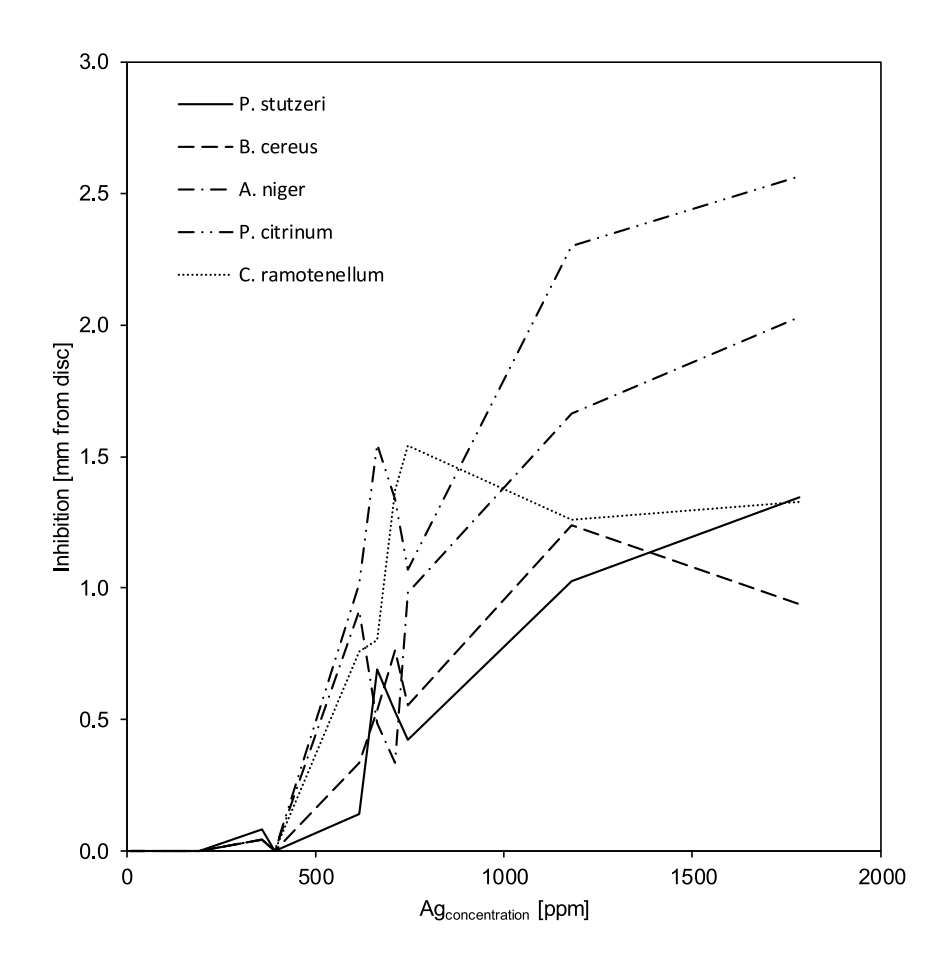


Fig. 5. Inhibition vs. Ag concentration for individual microbial strains.

If antimicrobial activity is mainly associated with silver ion release, a linear relationship between normalized silver concentration and normalized inhibition should be observed. Therefore, we plotted the normalized values, excluding data points below the minimum silver

concentration threshold required for inhibition and those within the plateau region – which we previously hypothesized to be influenced by the balance between diffusion and microbial growth dynamics (Fig. 6) ("Inhibition vs. Ag concentration", Supporting information 1).

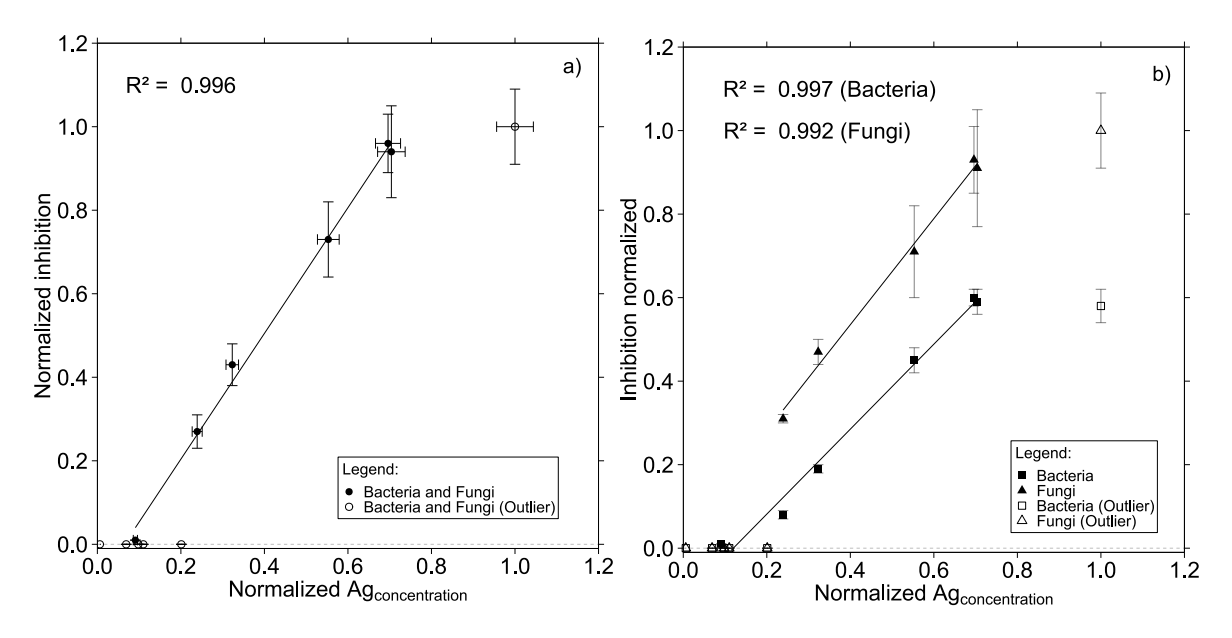


Fig. 6. Normalized silver concentration vs. normalized inhibition in disc diffusion assays.

Legend: a) all microorganisms; b) individual taxa; Both excluding outlier M2Ms5 and no measurable inhibition (n.i.) from Table 5.

The results provide compelling evidence and strongly support the hypothesis ( $R^2=0.996$  (all);  $R^2=0.997$  (bacteria);  $R^2=0.992$  (fungi)) that the inhibition observed in diffusion assays is predominantly governed by the silver ions release rate from nanoparticles. We did observe differences between profiles from bacteria and fungi (Fig. 6), which suggests that the antimicrobial mechanisms are not equivalent. This supports observations from previous studies and might be related to the distinct NPs internalization capabilities from eukaryotic and prokaryotic cells (Loza et al., 2014a).

# 3.2.5. Diffusion mechanism for Ag-based NPs in agar

Based on observations from both this study and others, we propose a mechanism for the  $\mathrm{Ag}^+$  release from Ag-based NPs and subsequent diffusion in antimicrobial diffusion assays (Fig. 7). A few studies (Ackers

and Steere, 1962; Pluen et al., 1999) have shown that for commonly used agar concentrations ( $\sim$ 1.5 %, m/v), the diffusion of molecules within the size range of larger NPs will be negligible and others have shown that Ag<sup>+</sup> is released from Ag-based NPs. Silver ion (Ag<sup>+</sup>) release from AgNPs depends on dissolved O<sub>2</sub> (Loza et al., 2014a), whereas Ag<sup>+</sup> release form AgClNPs appears to rely on light exposure (Li et al., 2024). In this study we have shown that the model for Ag<sup>+</sup> release developed by Zhan et al. (Zhang et al., 2011) applies to disc diffusion assays of Ag-based NPs. Consequently, we proved that the antimicrobial activity determined with these tests is governed by the Ag<sup>+</sup> release rate rather than the diffusion of NPs. Additionally, Loza et al. have also shown that while dispersed in liquid biological media, Ag is mostly present as colloidal AgClNPs due to the reaction between the free Cl<sup>-</sup> present in the media and the released Ag<sup>+</sup> (Loza et al., 2014a, 2014b; Loza and Epple,

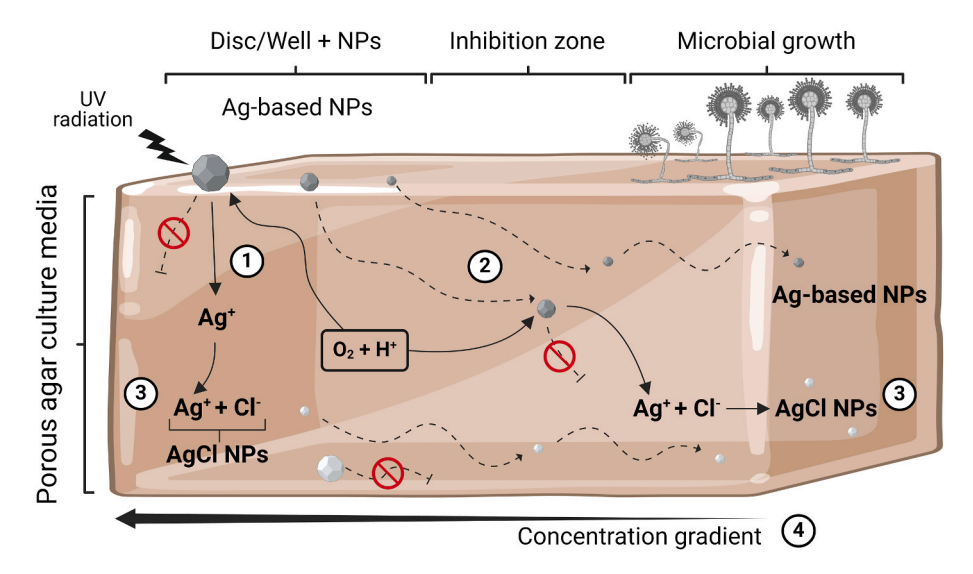


Fig. 7. Proposed simplified mechanisms of diffusion of  $Ag^+$  and Ag-based NPs in agar culture media. Legend: Dashed lines: NPs diffusion and interactions; Solid lines: ions and molecules diffusion and interactions; Gradient arrow pointing from lower to higher concentrations of Ag;  $\odot$ : impaired NPs diffusion due to size. 1) AgNPs release  $Ag^+$  upon oxidation by dissolved  $O_2$  and  $H^+$  while AgClNPs release  $Ag^+$  by interaction with UV-radiation; 2) The smallest NPs can diffuse through the agar pores; 3) Released  $Ag^+$  readily react with free  $Cl^-$  ions present in the culture medium to form AgClNPs; 4) These interactions, mainly dependent on  $Ag^+$  release form NPs, form a concentration gradient that, at high enough concentrations, inhibits microbial growth. (Created with BioRender.com)

2018). We propose that this should also occur in "solid" culture media because agar culture media is in fact a hydrogel composed of solid (agar) and liquid (culture media) phases. As Armisén and Gaiatas explain, agar is known to produce "physical gels" which means that all their structure is formed only by the polymer molecules which aggregate through hydrogen bonds, resulting in gelling properties that allow them to hold a great amount of water which can move more freely (Armisén and Gaiatas, 2009). In fact, it has been shown that the water potential in liquid culture media is just marginally lower than in agar media (Aujla and Paulitz, 2017), and that the free diffusion of molecules such as NaCl – at low concentrations ( $\sim$ 50 mm), low agar % ( $\sim$ 1–3 %, m/v), and common incubation temperatures (25–35 °C) – is not significantly reduced (Fujii and Thomas, 1958), meaning that for small molecules ( $\ll$  agar pore) and ions, diffusion rate is not significantly affected and the observations and reactions from liquid media should apply to agar media as well.

### 4. Conclusions

We have successfully synthesized Ag-based NPs by adding AgNO<sub>3</sub> to supernatants of microbial cultures. These nanoparticles showed high bacteriostatic/fungistatic antimicrobial potential, with MIC values mostly ranging from 3 to 28 ppm against microbial isolates from cultural heritage materials, whereas a 10-fold increase in concentration was generally required for lethal activity to be observed. Kinetic analysis of disc diffusion results, using a model for Ag release from NPs (Zhang et al., 2011), revealed for the first time, to the best of our knowledge, that inhibition zones are directly proportional to silver ion release rates from nanoparticles rather than their direct diffusion in agar. Additionally, the sigmoidal profile observed between inhibition zones and Ag concentration suggests that these zones result from a complex balance between silver release kinetics, the diffusion rate of agar-formed AgClNPs, and microbial growth rates. Together, these observations challenge the effectiveness of the disc diffusion method for evaluating nanoparticle antimicrobial activity and support the concerns raised in previous studies (Gopal et al., 2018; Kourmouli et al., 2018; Loza et al., 2014a). These findings also led to the proposal of a simplified mechanism for diffusion assays of Ag-based NPs. Despite its widespread use, disc diffusion assays prove inadequate for directly assessing the antimicrobial effects of nanoparticles, as it primarily reflects the balance between microbial growth kinetics and the diffusion dynamics of AgClNPs formed through complex ion-media interactions. Therefore, given the strong antimicrobial potential of biosynthesized Ag-based NPs, particularly against CH-associated microorganisms, it is critical to adopt and standardize alternative evaluation techniques. Additionally, these findings carry broad implications beyond CH conservation, extending into human health, medicine, and biotechnology - fields in which accurate assessment of nanoparticle antimicrobial efficacy is paramount for both clinical and industrial applications. Methods such as colony counts on agar-spread nanoparticles offer alternative approaches to accurately measure nanoparticle activity and should be further explored to replace diffusion-based assays.

# CRediT authorship contribution statement

António Carrapiço: Writing – review & editing, Writing – original draft, Visualization, Validation, Methodology, Investigation, Formal analysis, Conceptualization. Manuel Pico: Writing – review & editing, Investigation. Elisabete P. Carreiro: Writing – review & editing, Resources, Methodology. Pedro Barrulas: Writing – review & editing, Validation, Resources, Methodology. José Mirão: Writing – review & editing, Resources, Funding acquisition. Ana Teresa Caldeira: Writing – review & editing, Resources, Funding acquisition. Jorge Teixeira: Writing – review & editing, Supervision, Resources. Luís Dias: Writing – review & editing, Validation, Supervision, Resources, Funding acquisition, Conceptualization. Maria Rosario Martins: Writing – review & editing, Validation, Supervision, Resources.

#### Ethics approval and consent to participate

Not applicable.

# Consent for publication

Not applicable.

### **Funding sources**

This research was funded by Fundação para a Ciência e Tecnologia (FCT) under the multi-annual financing projects (2020–2023) UIDB/04449/2020 (doi:10.54499/UIDB/04449/2020) and UIDP/04449/2020 (doi:10.54499/UIDP/04449/2020), with research grant number UI/BD/153583/2022, under the collaboration protocol agreed between the FCT and HERCULES Laboratory for the financing of student doctorate research, and employment contract 2023.06272.CEECIND/CP2849/CT0001; by the IN2PAST Associated Laboratory under the project LA/P/0132/2020 (doi:10.54499/LA/P/0132/2020), and by the project "Sustainable Stone by Portugal—Valorization of Natural Stone for a digital, sustainable and qualified future", n° 40, proposal n° C644943391-00000051, co-financed by PRR-Recovery and Resilience Plan of the European Union (Next Generation EU).

### **Declaration of competing interest**

The authors declare that they have no known competing financial interests or personal relationships that could have appeared to influence the work reported in this paper.

### Acknowledgments

To Fundação para a Ciência e Tecnologia (FCT), IN2PAST Associated Laboratory, HERCULES Laboratory, and the University of Évora, for financing the doctorate research where this review is inserted. To the project "Sustainable Stone by Portugal—Valorization of Natural Stone for a digital, sustainable and qualified future", n° 40, proposal n° C644943391-00000051, co-financed by PRR—Recovery and Resilience Plan of the European Union (Next Generation EU). To FCT for the support provided through the LAQV-REQUIMTE projects UIDB/50006/2020 and UIDP/50006/2020, funded by Portuguese national funds.

# Appendix A. Supplementary data

Supplementary data to this article can be found online at https://doi.org/10.1016/j.ibiod.2025.106167.

# Data availability

The datasets used and analyzed during the current study are available in the Supporting information.

### References

- Ackers, G.K., Steere, R.L., 1962. Restricted diffusion of macromolecules through agar-gel membranes. Biochim. Biophys. Acta 59, 137–149. https://doi.org/10.1016/0006-3002(62)90704-7
- Al-Harbi, N., Abd-Elrahman, N.K., 2024. Physical methods for preparation of nanomaterials, their characterization and applications: a review. JUmm Al-Qura Univ Appll Sci. https://doi.org/10.1007/s43994-024-00165-7.
- Ali, A.Y., Alani, A.-A.K., Ahmed, B.O., Hamid, L.L., 2024. Effect of biosynthesized silver nanoparticle size on antibacterial and anti-biofilm activity against pathogenic multidrug resistant bacteria. OpenNano 20, 100213. https://doi.org/10.1016/j. opano 2024 100213
- Alotaibi, A.M., Alsaleh, N.B., Aljasham, A.T., Tawfik, E.A., Almutairi, M.M., Assiri, M.A., Alkholief, M., Almutairi, M.M., 2022. Silver nanoparticle-based combinations with antimicrobial agents against antimicrobial-resistant clinical isolates. Antibiotics 11, 1219. https://doi.org/10.3390/antibiotics11091219.

- Altomare, A., Corriero, N., Cuocci, C., Falcicchio, A., Moliterni, A., Rizzi, R., 2015. QUALX2.0: a qualitative phase analysis software using the freely available database POW\_COD. J. Appl. Crystallogr. 48, 598–603. https://doi.org/10.1107/ \$1600576715002319
- Armisén, R., Gaiatas, F., 2009. Agar. Handbook of Hydrocolloids. Elsevier, pp. 82–107. https://doi.org/10.1533/9781845695873.82.
- Aujla, İ.S., Paulitz, T.C., 2017. An improved method for establishing accurate water potential levels at different temperatures in growth media. Front. Microbiol. 8, 1497. https://doi.org/10.3389/fmicb.2017.01497.
- Berkow, E.L., Lockhart, S.R., Ostrosky-Zeichner, L., 2020. Antifungal susceptibility testing: current approaches. Clin. Microbiol. Rev. 33, e00069. https://doi.org/ 10.1128/CMR.00069-19
- Bernardes, L.M.M., Malta, S.M., Santos, A.C.C., Da Silva, R.A., Rodrigues, T.S., Da Silva, M.N.T., Bittar, V.P., Borges, A.L.S., Justino, A.B., Nossol, A.B.D.S., Martins, M. M., Espíndola, F.S., Mendes-Silva, A.P., Ueira-Vieira, C., 2025. Green synthesis, characterization, and antimicrobial activity of silver nanoparticles from water-soluble fractions of Brazilian kefir. Sci. Rep. 15, 10626. https://doi.org/10.1038/s11508.075.05616.4
- Bhattacharya, S., Acharya, A., 2020. Experimental Tools for Characterizations of Glass Nanocomposites Containing Metal Oxides. Metal Oxide Glass Nanocomposites. Elsevier, pp. 51–75. https://doi.org/10.1016/B978-0-12-817458-6.00004-4.
- Camuffo, D., Fassina, V., Havermans, J., 2010. Basic Environmental Mechanisms: Affecting Cultural Heritage; Understanding Deterioration Mechanisms for Conservation Purposes. Nardini, Firenze.
- Carrapiço, A., Martins, M.R., Caldeira, A.T., Mirão, J., Dias, L., 2023. Biosynthesis of metal and metal oxide nanoparticles using microbial cultures: mechanisms, antimicrobial activity and applications to cultural heritage. Microorganisms 11. https://doi.org/10.3390/microorganisms11020378.
- Dias, L., 2020. STONECOLOR: Color of Commercial Marbles and Limestone: Causes and Changes. PhD thesis in Biochemistry. University of Évora. http://hdl.handle.net/10 174/26969.
- CLSI (Ed.), 2014. Performance Standards for Antimicrobial Susceptibility Testing: Twenty-Forth Informational Supplement. Clinical and Laboratory Standards Institute, Wayne, PA.
- Doebelin, N., Kleeberg, R., 2015. Profex: a graphical user interface for the rietveld refinement program BGMN. J. Appl. Crystallogr. 48, 1573–1580. https://doi.org/ 10.1107/S1600576715014685.
- Einstein, A., 1905. Über die von der molekularkinetischen Theorie der Wärme geforderte Bewegung von in ruhenden Flüssigkeiten suspendierten Teilchen. Ann. Phys. 322, 549–560. https://doi.org/10.1002/andp.19053220806.
- Elwakil, B.H., Eldrieny, A.M., Almotairy, A.R.Z., El-Khatib, M., 2024. Potent biological activity of newly fabricated silver nanoparticles coated by a carbon shell synthesized by electrical arc. Sci. Rep. 14, 5324. https://doi.org/10.1038/s41598-024-54648-y.
- Espinel-Ingroff, A., 2007. Standardized disk diffusion method for yeasts. Clin. Microbiol. Newsl. 29, 97–100. https://doi.org/10.1016/j.clinmicnews.2007.06.001.
- Espinel-Ingroff, A., Canton, E., Fothergill, A., Ghannoum, M., Johnson, E., Jones, R.N., Ostrosky-Zeichner, L., Schell, W., Gibbs, D.L., Wang, A., Turnidge, J., 2011. Quality control guidelines for amphotericin B, itraconazole, posaconazole, and voriconazole disk diffusion susceptibility tests with nonsupplemented mueller-hinton agar (CLSI M51-A document) for nondermatophyte filamentous fungi. J. Clin. Microbiol. 49, 2568-2571. https://doi.org/10.1128/JCM.00393-11.
- Espinel-Ingroff, A., Cantón, E., Pemán, J., 2012. Antifungal susceptibility testing of filamentous fungi. Curr. Fungal. Infect. Rep. 6, 41–50. https://doi.org/10.1007/ s12281-011-0079-1
- Franco-Castillo, I., Hierro, L., de la Fuente, J.M., Seral-Ascaso, A., Mitchell, S.G., 2021. Perspectives for antimicrobial nanomaterials in cultural heritage conservation. Chem 7, 629–669. https://doi.org/10.1016/j.chempr.2021.01.006.
- Fujii, T., Thomas, H.C., 1958. Self-diffusion of sodium ion in agar gels. J. Phys. Chem. 62, 1566–1568. https://doi.org/10.1021/j150570a024.
- Gopal, J., Chun, S., Anthonydhason, V., Jung, S., Mwang'ombe, B.N., Muthu, M., Sivanesan, I., 2018. Assays evaluating antimicrobial activity of nanoparticles: a myth buster. J. Cluster Sci. 29, 207–213. https://doi.org/10.1007/s10876-018-1334-1.
- Gražulis, S., Chateigner, D., Downs, R.T., Yokochi, A.F.T., Quirós, M., Lutterotti, L., Manakova, E., Butkus, J., Moeck, P., Le Bail, A., 2009. Crystallography open database – an open-access collection of crystal structures. J. Appl. Crystallogr. 42, 726–729. https://doi.org/10.1107/S0021889809016690.
- Greulich, C., Braun, D., Peetsch, A., Diendorf, J., Siebers, B., Epple, M., Köller, M., 2012. The toxic effect of silver ions and silver nanoparticles towards bacteria and human cells occurs in the same concentration range. RSC Adv. 2, 6981. https://doi.org/ 10.1039/c2ra20684f.
- Han, Z., Teah, H.Y., Hirasawa, I., Kikuchi, Y., 2025. Prospective life cycle assessment of emerging silver nanoparticle synthesis methods: one-Pot polyethyleneimine chemical reduction and biological reductions. J. Clean. Prod. 494, 145012. https:// doi.org/10.1016/j.jclepro.2025.145012.
- Holubnycha, V., Husak, Y., Korniienko, V., Bolshanina, S., Tveresovska, O., Myronov, P., Holubnycha, M., Butsyk, A., Borén, T., Banasiuk, R., Ramanavicius, A., Pogorielov, M., 2024. Antimicrobial activity of two different types of silver nanoparticles against wide range of pathogenic bacteria. Nanomaterials 14, 137. https://doi.org/10.3390/nano14020137.
- Jagdeo, K.R., 2023. Physical Methods for Synthesis of Nanoparticles. Nanochemistry, first ed. CRC Press, Boca Raton, pp. 66–76. https://doi.org/10.1201/ 9781003081944-4
- Kamer, A.M.A., El Maghraby, G.M., Shafik, M.M., Al-Madboly, L.A., 2024. Silver nanoparticle with potential antimicrobial and antibiofilm efficiency against multiple drug resistant, extensive drug resistant Pseudomonas aeruginosa clinical isolates. BMC Microbiol. 24, 277. https://doi.org/10.1186/s12866-024-03397-z.

- Khan, I., Saeed, K., Khan, I., 2019. Nanoparticles: properties, applications and toxicities. Arab. J. Chem. 12, 908–931. https://doi.org/10.1016/j.arabjc.2017.05.011.
- Kifle, D., Bacha, K., Gonfa, G., 2025. Antimicrobial activities of biosynthesized nanosilver using Musa paradisiaca and citrus sinensis peel extracts against major human and plant pathogens. Sci. Rep. 15, 6600. https://doi.org/10.1038/s41598-025-91020-0.
- Kourmouli, A., Valenti, M., Van Rijn, E., Beaumont, H.J.E., Kalantzi, O.-I., Schmidt-Ott, A., Biskos, G., 2018. Can disc diffusion susceptibility tests assess the antimicrobial activity of engineered nanoparticles? J. Nano Res. 20, 62. https://doi.org/10.1007/s11051-018-4152-3.
- Lafuente, B., Downs, R.T., Yang, H., Stone, N., 2015. 1. The power of databases: the RRUFF project. In: Armbruster, T., Danisi, R.M. (Eds.), Highlights in Mineralogical Crystallography. DE GRUYTER, pp. 1–30. https://doi.org/10.1515/ 9783110417104-003.
- Li, X., Zhou, Y., Feng, X., 2024. Superior photocatalytic activity and antibacterial behavior of chitosan-anchored Ag/AgCl composites. Water Air Soil Pollut. 235, 103. https://doi.org/10.1007/s11270-023-06870-z.
- Lima, A.K.O., Souza, L.M.D.S., Reis, G.F., Junior, A.G.T., Araújo, V.H.S., Santos, L.C.D., Silva, V.R.P.D., Chorilli, M., Braga, H.D.C., Tada, D.B., Ribeiro, J.A.D.A., Rodrigues, C.M., Nakazato, G., Muehlmann, L.A., Garcia, M.P., 2024. Synthesis of silver nanoparticles using extracts from different parts of the Paullinia cupana kunth plant: characterization and in vitro antimicrobial activity. Pharmaceuticals 17, 869. https://doi.org/10.3390/ph17070869.
- Loza, K., Epple, M., 2018. Silver nanoparticles in complex media: an easy procedure to discriminate between metallic silver nanoparticles, reprecipitated silver chloride, and dissolved silver species. RSC Adv. 8, 24386–24391. https://doi.org/10.1039/ C8RA04500C.
- Loza, K., Diendorf, J., Sengstock, C., Ruiz-Gonzalez, L., Gonzalez-Calbet, J.M., Vallet-Regi, M., Köller, M., Epple, M., 2014a. The dissolution and biological effects of silver nanoparticles in biological media. J. Mater. Chem. B 2, 1634. https://doi.org/10.1039/c3tb21569e.
- Loza, K., Sengstock, C., Chernousova, S., Köller, M., Epple, M., 2014b. The predominant species of ionic silver in biological media is colloidally dispersed nanoparticulate silver chloride. RSC Adv. 4, 35290. https://doi.org/10.1039/C4RA04764H.
- Malvern Panalytical, 2021. Zetasizer Software v8-02. https://www.malvernpanalytical.com/en/support/product-support/software/zetasizer-family-software-update
- Menichetti, A., Mavridi-Printezi, A., Mordini, D., Montalti, M., 2023. Effect of size, shape and surface functionalization on the antibacterial activity of silver nanoparticles. J. Forensic Biomech. 14, 244. https://doi.org/10.3390/jfb14050244.
- Monopoli, M.P., Walczyk, D., Campbell, A., Elia, G., Lynch, I., Baldelli Bombelli, F., Dawson, K.A., 2011. Physical—Chemical aspects of protein Corona: relevance to in Viro and in Vivo biological impacts of nanoparticles. J. Am. Chem. Soc. 133, 2525–2534. https://doi.org/10.1021/ia107583h.
- Morone, M.V., Chianese, A., Dell'Annunziata, F., Folliero, V., Lamparelli, E.P., Della Porta, G., Zannella, C., De Filippis, A., Franci, G., Galdiero, M., Morone, A., 2024. Ligand-Free silver nanoparticles: an innovative strategy against viruses and bacteria. Microorganisms 12, 820. https://doi.org/10.3390/microorganisms12040820.
- Narayanan, K.B., Sakthivel, N., 2010. Biological synthesis of metal nanoparticles by microbes. Adv. Colloid Interface Sci. 156, 1–13. https://doi.org/10.1016/j. cis.2010.02.001.
- Newbury, D.E., Ritchie, N.W.M., 2022. Energy-dispersive X-Ray spectrum simulation with NIST DTSA-II: comparing simulated and measured electron-excited spectra. Microsc. Microanal. 28, 1905–1916. https://doi.org/10.1017/S1431927622012272.
- Nunes, P., 2017. Estudo de Comunidades Microbianas Presentes em Amostras Arqueológicas. MSc dissertation in Biochemistry. University of Évora. http://hdl.han dle.net/10174/21806.
- Ogochukwu, O.O., Fabiyi, M.B., Aworunse, O.S., Oyewole, O.A., Isibor, P.O., 2024.
  Nanoparticle properties and characterization. In: Isibor, P.O., Devi, G., Enuneku, A.
  A. (Eds.), Environmental Nanotoxicology. Springer Nature Switzerland, Cham,
  pp. 23–40. https://doi.org/10.1007/978-3-031-54154-4\_2.
- Pérez-Hernández, H., Pérez-Moreno, A., Sarabia-Castillo, C.R., García-Mayagoitia, S., Medina-Pérez, G., López-Valdez, F., Campos-Montiel, R.G., Jayanta-Kumar, P., Fernández-Luqueño, F., 2021. Ecological drawbacks of nanomaterials produced on an industrial Scale: collateral effect on human and environmental health. Water Air Soil Pollut. 232, 435. https://doi.org/10.1007/s11270-021-05370-2.
- Pluen, A., Netti, P.A., Jain, R.K., Berk, D.A., 1999. Diffusion of macromolecules in agarose gels: comparison of linear and globular configurations. Biophys. J. 77, 542–552. https://doi.org/10.1016/S0006-3495(99)76911-0.
- Posit team, 2024. Rstudio: Integrated Development Environment for R.Posit Software.

  PBC, Boston, MA. https://www.scirp.org/reference/referencespapers?reference
  id=3810421
- Pourzahedi, L., Eckelman, M.J., 2015. Comparative life cycle assessment of silver nanoparticle synthesis routes. Environ. Sci. Nano 2, 361–369. https://doi.org/ 10.1039/C5EN00075K.
- Ritchie, N.W.M., 2009. Spectrum simulation in DTSA-II. Microsc. Microanal. 15, 454–468. https://doi.org/10.1017/S1431927609990407.
- Ritchie, N.W.M., Newbury, D.E., Davis, J.M., 2012. EDS measurements of X-Ray intensity at WDS precision and accuracy using a silicon drift detector. Microsc. Microanal. 18, 892–904. https://doi.org/10.1017/S1431927612001109.
- Ritchie, N.W.M., Herzing, A., Oleshko, V.P., 2023. Quantification of unsupported thinfilm X-ray spectra using bulk standards. Microsc. Microanal. 29, 1921–1930. https:// doi.org/10.1093/micmic/ozad109.
- Salvador, C., Letras, J., Candeias, A., Caldeira, A.T., 2023. In: Saccharomyces cerevisiae strain CCLBH-GMYXII large subunit ribosomal RNA gene, partial sequence. Genbank. National Library of Medicine (US), National Center for Biotechnology

- Information, Bethesda (MD). https://www.ncbi.nlm.nih.gov/nuccore/OR790557.1 (Accessed 3 July 2025).
- Salvador, C., Macedo-Arantes, S., Candeias, A., Caldeira, A.T., 1982. Penicillium citrinum strain CCLBH GSG1F1 internal transcribed spacer 1, partial sequence; 5.8S ribosomal RNA gene and internal transcribed spacer 2, complete sequence; and large subunit ribosomal RNA gene, partial sequenceGenbank. National Library of Medicine (US), National Center for Biotechnology Information, Bethesda (MD). https://www.ncbi.nlm.nih.gov/nuccore/OR836964.1. (Accessed 25 November 2024)
- Salvador, C., Macedo-Arantes, S., Candeias, A., Caldeira, A.T., 2023. In: Bacillus cereus strain CCLBH GSF11 16S ribosomal RNA gene, partial sequence. Genbank, National Library of Medicine (US), National Center for Biotechnology Information, Bethesda (MD). https://www.ncbi.nlm.nih.gov/nuccore/OR831969.1 (Accessed 25 November 2024).
- Schneider, C.A., Rasband, W.S., Eliceiri, K.W., 2012. NIH image to ImageJ: 25 years of image analysis. Nat. Methods 9, 671–675. https://doi.org/10.1038/nmeth.2089.
- Schwalbe, R., Steele-Moore, L., Goodwin, A.C. (Eds.), 2007. Antimicrobial Susceptibility Testing Protocols, 0 ed. CRC Press. https://doi.org/10.1201/9781420014495.
- Sharma, V.K., Yngard, R.A., Lin, Y., 2009. Silver nanoparticles: green synthesis and their antimicrobial activities. Adv. Colloid Interface Sci. 145, 83–96. https://doi.org/ 10.1016/j.cis.2008.09.002.
- Stokes, G.G., 1851. On the effect of the internal friction of fluids on the motion of pendulums. Trans. Cambridge Philosoph. Soc. 9, 8.
- Temizel-Sekeryan, S., Hicks, A.L., 2020. Global environmental impacts of silver nanoparticle production methods supported by life cycle assessment. Resour. Conserv. Recycl. 156, 104676. https://doi.org/10.1016/j.resconrec.2019.104676.

- Thakkar, K.N., Mhatre, S.S., Parikh, R.Y., 2010. Biological synthesis of metallic nanoparticles. Nanomed. Nanotechnol. Biol. Med. 6, 257–262. https://doi.org/ 10.1016/j.nano.2009.07.002.
- The European Committee on Antimicrobial Susceptibility Testing, 2023. Antimicrobial Susceptibility Testing EUCAST Disk Diffusion Method.
- The European Council, 2006. Council of Europe Framework Convention on the Value of Cultural Heritage for Society: Faro 27. X. 2005 aÉd. du Conseil de l'Europe.
- UNESCO, 1972. UNESCO Convention Concerning the Protection of the World Cultural and Natural Heritage. https://whc.unesco.org/en/conventiontext/.
- Vaitkus, A., Merkys, A., Gražulis, S., 2021. Validation of the crystallography open database using the crystallographic information framework. J. Appl. Crystallogr. 54, 661–672. https://doi.org/10.1107/S1600576720016532.
- Vishwanath, R., Negi, B., 2021. Conventional and green methods of synthesis of silver nanoparticles and their antimicrobial properties. Curr. Res. Green Sustain. Chem. 4, 100205. https://doi.org/10.1016/j.crgsc.2021.100205.
- Wang, Y., Zhai, W., Li, J., Liu, H., Li, C., Li, J., 2023. Friction behavior of biodegradable electrospun polyester nanofibrous membranes. Tribol. Int. 188, 108891. https://doi. org/10.1016/j.triboint.2023.108891.
- Ying, S., Guan, Z., Ofoegbu, P.C., Clubb, P., Rico, C., He, F., Hong, J., 2022. Green synthesis of nanoparticles: current developments and limitations. Environ. Technol. Innovat. 26, 102336. https://doi.org/10.1016/j.eti.2022.102336.
- Zhang, W., Yao, Y., Sullivan, N., Chen, Y., 2011. Modeling the primary size effects of citrate-coated silver nanoparticles on their ion release kinetics. Environ. Sci. Technol. 45, 4422–4428. https://doi.org/10.1021/es104205a.
- Zhang, X.-F., Liu, Z.-G., Shen, W., Gurunathan, S., 2016. Silver nanoparticles: synthesis, characterization, properties, applications, and therapeutic approaches. IJMS 17, 1534. https://doi.org/10.3390/ijms17091534.
- Zhang, Y., Liu, X., Luo, J., Liu, H., Li, Y., Liu, J., Zhu, L., Wang, J., Zeng, H., 2025. Dual recombinase polymerase amplification system combined with lateral flow immunoassay for simultaneous detection of Staphylococcus aureus and Vibrio parahaemolyticus. J. Pharmaceut. Biomed. Anal. 255, 116621. https://doi.org/10.1016/j.jpba.2024.116621.